

Review

Progress of Electrical Resistance Tomography Application in Oil and Gas Reservoirs for Development Dynamic Monitoring

Wenyang Shi ^{1,*} , Guangzhi Yin ¹, Mi Wang ^{2,*}, Lei Tao ¹, Mengjun Wu ¹, Zhihao Yang ¹, Jiajia Bai ¹, Zhengxiao Xu ¹ and Qingjie Zhu ¹

¹ School of Petroleum and Natural Gas, Changzhou University, Changzhou 213164, China; 0950gjk459@163.com (G.Y.)

² School of Chemical and Process Engineering, University of Leeds, Leeds LS2 9JT, UK

* Correspondence: w.shi@cczu.edu.cn (W.S.); m.wang@leeds.ac.uk (M.W.)

Abstract: Petroleum engineers need real-time understanding of the dynamic information of reservoirs and production in the development process, which is essential for the fine description of oil and gas reservoirs. Due to the non-invasive feature of electromagnetic waves, more and more oil and gas reservoirs have received attention to capture the development dynamics with electrical resistance tomography (ERT). By measuring the distribution of resistivity on the surface, the ERT can offer information on the subsurface media. The theory and foundation of the ERT technology are presented in this study in the context of monitoring oil and gas reservoir growth dynamics. The characteristics of ERT technology are analyzed, and the progress of ERT application in the development of monitoring dynamics in terms of residual oil distribution, detection of water-driven leading edge, and monitoring of fractures during hydraulic fracturing is reviewed, as well as the progress of ERT technology optimization, including forward and inverse algorithms. This review aims to promote further application of ERT in the field of reservoir dynamics monitoring because of its important engineering significance as well as its academic value in terms of improving production efficiency and reducing risk.



Citation: Shi, W.; Yin, G.; Wang, M.; Tao, L.; Wu, M.; Yang, Z.; Bai, J.; Xu, Z.; Zhu, Q. Progress of Electrical Resistance Tomography Application in Oil and Gas Reservoirs for Development Dynamic Monitoring. *Processes* **2023**, *11*, 2950. <https://doi.org/10.3390/pr11102950>

Academic Editor: Mohd Azlan Hussain

Received: 15 August 2023
Revised: 28 September 2023
Accepted: 7 October 2023
Published: 11 October 2023



Copyright: © 2023 by the authors. Licensee MDPI, Basel, Switzerland. This article is an open access article distributed under the terms and conditions of the Creative Commons Attribution (CC BY) license (<https://creativecommons.org/licenses/by/4.0/>).

Keywords: tomography; residual oil distribution; waterflooding front; hydraulic fracture; inverse algorithms

1. Introduction

Monitoring the dynamics of oil and gas reservoir development can provide in-time information about the reservoir and provide key data support for reservoir engineers. Accurate monitoring results can provide an in-depth understanding of the dynamic changes, reserve distribution, fluid migration, and other characteristics of the reservoir to maximize the development and utilization of oil and gas resources, reduce the development risk, and improve the recovery rate and production. Therefore, monitoring the dynamics of oil and gas reservoir development is of great importance in oil and gas exploration and exploitation. Electrical Resistance Tomography (ERT), as a non-invasive and real-time subsurface imaging technology, occupies a key position in the process of monitoring the dynamics of oil and gas reservoir development. Its successful application in the field of monitoring the dynamics of oil and gas reservoir development has been recognized by many experts and researchers [1–3].

ERT is a multidisciplinary real-time online detection technology that meets the needs of actual industrial production and has been widely used in the fields of chemical engineering industry [4], environment and pollution [5,6], biomedical and pharmaceutical [7], biological and ecology [8], new energy [9], and marine development [10,11]. The origin of Electrical Resistance Tomography (ERT) can be traced back to the resistivity imaging of linear electrode arrays proposed in the 1920s [12], and the concept of “flow imaging” and

the technique of “process tomography” were proposed by a research team at the University of Manchester, UK, in 1985 [13], which laid the foundation for modern industrial chromatography. Currently, the widely used and mature technology of Electrical Impedance Tomography (EIT) includes Electrical Capacitance Tomography (ECT) [14], Electrical Resistance Tomography (ERT [15,16], and Electromagnetic Tomography (EMT) [17,18]. In the 1990s, ERT was rapidly expanded into the industrial field, where it is used in groundwater resource management, environmental monitoring, monitoring pipeline blockage and fluid distribution in petrochemicals, and detection of underground CO₂ transport [19–22].

Potentiometric testing has been utilized in the oilfield since the mid- to late-1900s. Meanwhile, ERT technology has been gradually applied to the dynamic monitoring of oil and gas reservoirs and verified in actual oilfields. The well-known Sandia Laboratories in the U.S.A. used this technique to evaluate the asymmetry of fractures and to detect the orientation of hydraulically fractured fractures, among other things [23]. Ref. [24] used this method to find a high abundance of dead oil zones in several lithologic traps in an oil-bearing region of the former Soviet Union. Ref. [25] used this method to identify the depth of burial and the distribution of geothermal reservoirs in a regional hot field. [26] used this method to effectively monitor oil and gas reservoirs in terms of the direction of the hot-water tongue and the advancement of water injection. Ref. [27] investigated the flow process during water displacement of oil in a sand-filled model using a low-field ERT basis indoors, which demonstrates the promising application of ERT for monitoring the dynamics of porous media.

At the beginning of the 21st century, with the advancement of computer technology and data processing algorithms, ERT technology has been further improved in monitoring the dynamics of oil and gas reservoir development. In China, ERT has been utilized in many oilfields such as Shengli, Daqing, and Changqing, with a total of more than 400 times, and the construction failure rate is 0% [28]. Through field exploration and experimentation, researchers have verified the feasibility and effectiveness of ERT in monitoring the dynamics of oil and gas reservoir development [29,30]. High-resolution data acquisition equipment, advanced imaging algorithms, and real-time monitoring systems enable ERT to provide more accurate and faster acquisition and analysis of reservoir information. In recent years, ERT has often been used in combination with other monitoring techniques to obtain more comprehensive reservoir information. Through the comprehensive application of multiple monitoring means, accurate monitoring and evaluation of key parameters such as reservoir dynamic changes, flooding effect, and oil-water interface can be realized [31–33].

This paper mainly reviews the current research status and application progress of ERT technology in monitoring the dynamics of oil and gas reservoir development and gives an outlook on its future development. It has important engineering significance and academic value for promoting the application research of ERT in dynamic monitoring of oil and gas reservoir development, discovering the prospects and potential technological breakthroughs for the application of ERT technology in the field of dynamic monitoring of oil and gas reservoir development, and improving the extraction efficiency and reducing the risk.

2. Principles of Electrical Resistive Tomography and Comparison with Other Dynamic Monitoring Technologies for Reservoir Development

2.1. ERT Technology

Based on the spatial scale of the test and the magnitude of the excitation electric field, ERT can be classified into high-intensity field ERT and low-intensity field ERT. Both high-intensity field ERT and low-intensity field ERT technology are based on the basic principle of dielectric resistivity differences, with the former being suitable for wide-area measurements in the field and the latter for indoor measurements. Typically, a current is first introduced into the medium by a power supply, and then the potential distribution in the subsurface or sample is measured using electrodes. The ultimate goal is to create images or models representing resistivity distributions through inversion algorithms that

can be used to infer subsurface structures, geologic features, or the nature of the samples being studied. Interpretation of these images helps researchers make informed decisions in various applications.

2.1.1. Low-Field ERT

Low-field ERT, also known as industrial ERT, is mainly used for monitoring fluids in conventional sewers, etc. The low-field ERT system consists of four main parts: a sensor array unit, a data acquisition and processing unit, an image reconstruction unit, and a main control computer [34]. As shown in Figure 1, the 16-sensor electrode array and the excitation system are arranged equidistantly in the outer ring of the tubular space, which together form the spatially sensitive array unit. First, the host computer sends commands to the data acquisition and processing unit, and under the microcurrent (1–15 mA) excitation of any adjacent electrodes (e.g., 1–16 electrode pairs), the change of the conductivity field causes the change of the potential difference of the remaining 13 electrode pairs (e.g., 3–4 electrode pairs), which is the excitation process of the electrode pairs at one time. The excitation process of the remaining 14 adjacent electrode pairs is passed through a high frequency switching circuit (Figure 1a). Theoretically, a complete excitation cycle produces 16×13 measured potential values, but in practice, 104 measured potential values are sufficient for the traversal test according to the reciprocity theorem [35].

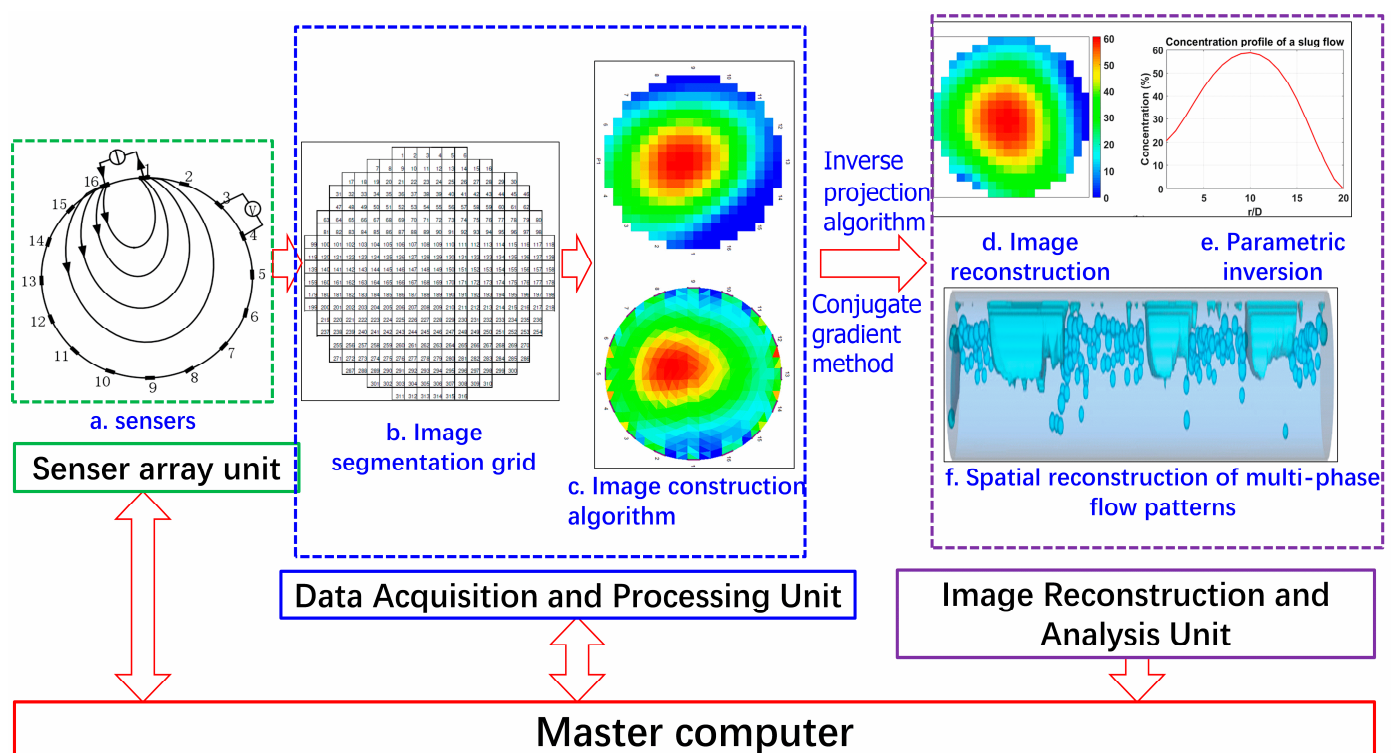


Figure 1. Low-Field ERT System (adapted from literature [35,36]).

Second, the data acquisition and processing unit (Figure 1b) demodulates and filters the measured potential values. Finally, the image reconstruction algorithm (Figure 1c) realizes functions such as cross-sectional image reconstruction (Figure 1d), flow parameter inversion (Figure 1e), and spatial reconstruction of the flow pattern (Figure 1f).

2.1.2. High-Field ERT

High-field ERT, also called well-ground ERT, as shown in Figure 2, one test well (A) was selected to inject current, and another well (B) was selected as a current-return well. On the surface of the tested well, 18×8 electrodes were buried and constructed into multi-electrode arrays (Figure 2a). The current flows from the test well and through the

rock or fluid of the oil reservoir and finally arrives at the return well to form a current loop (Figure 2b). The surface potential distribution of test well A is obtained from the test N potential data (Figure 2c), and then the resistivity distribution of the test formation is inverted by the image reconstruction algorithm (Figure 2d). Finally, the reservoir or fluid distribution characteristics are obtained, such as reservoir anomalies, flow boundaries, waterflood front edge (Figure 2e), and so on.

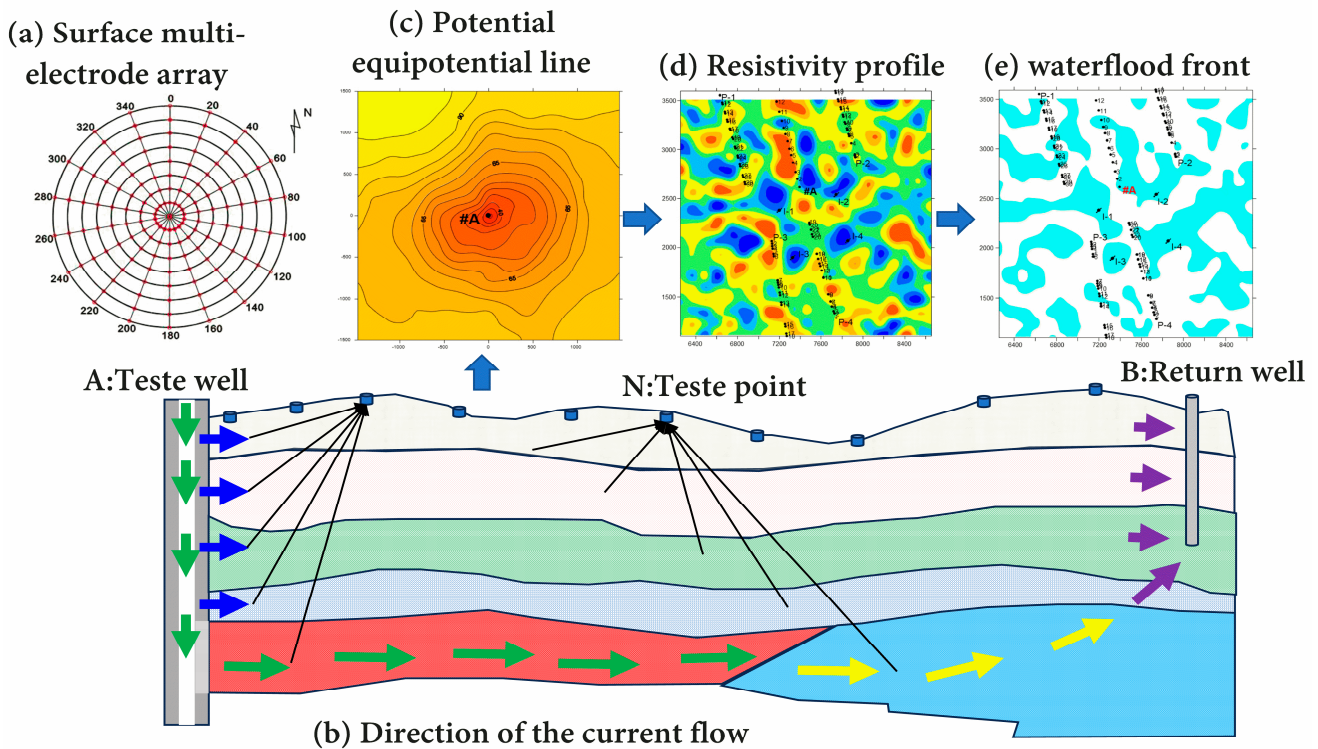


Figure 2. High-Field ERT System (adapted from literature [37,38]).

2.2. ERT Imaging Theory

2.2.1. Theory of Orthogonal Imaging

Orthorectification of the well-ground ERT system means that the distribution of resistivity parameters of the formation medium around the well is known and the potential distribution at the surface of the measurement system is calculated, which lays the foundation for the inversion and interpretation of the field measurement data. Orthorectification theory uses mathematical methods to describe the potential changes in the potential measurement system.

1. Basic analytical methods for line power fields

According to Maxwell's equation [39], the current source injects a current into the field, and the distribution of the electric field is determined by the current injected by the current source; therefore, for any point in the field, there is:

$$\nabla \cdot J = I\delta(r - r_s) \quad (1)$$

$$J = \sigma E \quad (2)$$

$$E = -\nabla\varphi \quad (3)$$

where, J is the current density, A/m ; I is current, A ; σ is the conductivity, S/m ; E is the electric field strength, V/m ; and φ is the potential, V . At the right end is the current source

term, δ is a Dirac function, and r and r_s are the positions of the observation point and the current source in m , respectively.

In the well-ground ERT method, the observed data obtained are the potential data of the ground surface. To eliminate the singularities in the vicinity of the source point and to improve the computational accuracy of the 3D orthogonal evolution, the singular value decomposition is generally used at present, i.e., the total potential is separated into background and anomalous potentials by the expression

$$\varphi = \varphi_p + \varphi_s \quad (4)$$

where, φ_p is the normal potential in V , which is the potential generated by the line source in the uniform half-space, and φ_s is the anomalous potential in V , which is generated by the current scattered by the anomalies and is obtained by using numerical calculations.

The total potential φ satisfies the following Poisson's equation, which describes the relationship between potential and conductivity under a steady current source.

$$\nabla \cdot (\sigma \nabla \varphi) = -I\delta(r - r_s) \quad (5)$$

Let the average conductivity of the borehole resistivity model be σ_m , in S/m , and φ_p satisfy the equation:

$$\nabla \cdot (\sigma_m \nabla \varphi_p) = -I\delta(r - r_s) \quad (6)$$

Substituting Equations (5) and (7) into (6) and eliminating the current source term, the differential equation for the anomalous potential φ_s is obtained as

$$\nabla(\sigma \nabla \varphi_s) = -\nabla \cdot [(\sigma - \sigma_m) \nabla \varphi_p] \quad (7)$$

2. Boundary condition

When solving the Poisson equation, appropriate boundary conditions must be specified. Boundary conditions are used to limit the solution domain and obtain an accurate potential response. The boundary conditions involved in well-ground ERT are as follows [40]:

(1) Dirichlet boundary conditions. The Dirichlet boundary condition is used to specify the exact value of the potential at the boundary.

$$\phi|_{\Gamma_n} = \text{constant}(n = 1, 2, \dots, N) \quad (8)$$

where Γ_1 and Γ_2 are current driving electrode domains (for example, an electrode domain for the adjacent electrode pair strategy or a metal-walled domain for conducting the boundary strategy), and N is the number of electrodes used in the strategy.

(2) Neumann boundary conditions.

(i) Relationship between the electric current density and the potential gradient across the measurement (voltage measurement) and the dielectric conductivity.

$$\sigma \frac{\partial \phi}{\partial n} \Big|_{\Gamma_1} = j_1(\Gamma_1), \quad \sigma \frac{\partial \phi}{\partial n} \Big|_{\Gamma_2} = j_2(\Gamma_2) \quad (9)$$

(ii) In the other boundary fields, the potential gradient has a value of 0 in the direction orthogonal to the equipotential line.

$$\frac{\partial \phi}{\partial n} \Big|_{\Pi} = 0 \quad (10)$$

where Π represents other domains at the boundary.

(3) Mixed boundary condition. This relationship states the relationship between the sinking current strength and the potential gradient and dielectric conductivity.

$$\int_{\Gamma_1} \sigma \frac{\partial \phi}{\partial n} d\Gamma = I, \int_{\Gamma_2} \sigma \frac{\partial \phi}{\partial n} d\Gamma = -I \quad (11)$$

3. Equation solving

To solve Poisson's equation, numerical calculation methods such as Finite Element Method (FEM), Finite Difference Method (FDM), or Analytical Method are commonly used. The following are two common numerical methods:

(1) Finite Element Method: The FEM is a commonly used numerical computational method for solving partial differential equations. In the FEM, the solution domain is divided into discrete finite elements, and the potential field within each finite element is approximated as a linear combination of a set of basic functions. These basis functions are usually localized and satisfy continuity conditions at the nodes. By constructing appropriate interpolation functions and basic functions on each finite element, the original Poisson equation can be transformed into a discretized set of algebraic equations. The most used solution methods are weighted residual methods in the FEM, such as the Weighted Residual method or the Galerkin method. By solving the system of algebraic equations, a numerical solution to the potential field can be obtained.

(2) Finite Difference [41,42] Method: The FDM is a common numerical calculation method that divides the solution domain into discrete grids, in which the derivatives in the partial differential equations are replaced by difference approximations. In the FDM, the numerical solution of the potential field is approximated at the mesh nodes. By approximating the derivative terms in the Poisson equation as differences at the mesh nodes, a series of algebraic equations can be obtained. These equations form a discretized system. By solving these equations iteratively, the numerical solution of the potential field can be computed step by step.

(3) Analytical Method: The Analytical Method is a mathematical method based on an analytical solution, in which a solution with a mathematical expression is obtained by analysis and derivation. However, in the actual well-ground ERT forward problem, it is difficult to obtain the analytical solution in the closed domain due to the complexity of the underground medium and the uncertainty of the boundary conditions. Therefore, the application of analytical methods in well-ground ERT normalization is more limited.

2.2.2. Theory of Inverse Imaging Theory

Resistivity three-dimensional inversion is the basis of the qualitative interpretation of the reservoir, according to the geological stratification of the geoelectric profile stratification and the depth of the geological stratification to determine the spatial distribution of resistivity and polarizability to carry out the interpretation of the reservoir. The inversion process is as follows.

(i) Calculate the apparent resistivity anomaly of the initial model and the residual difference between it and the measured apparent resistivity anomaly according to the 3D forward simulation method.

(ii) Calculate the Jacobi matrix A. The calculation of the Jacobi matrix is the most time-consuming, especially in the case of the 3D inverse problem, which has a large number of parameters, resulting in a long computation time and large storage capacity. Therefore, the least squares inverse convolution algorithm is used to solve this problem. In this algorithm, the average value of the full visual resistivity is used as the model for the forward computation, and the Jacobi term is used as the Jacobi term of the homogeneous model to achieve the high speed of the inverse computation.

(iii) Solve the linear least squares equation, Equation (12), to obtain the corrections to the parameters.

$$\left(A^T A + \lambda C^T C\right) \Delta P = A^T \Delta g \quad (12)$$

In the formula, A is the Jacobi term, the bias of the observations on the parameters of the model. C is a smoothing filter. λ is a damping factor. ΔP is the model parameter correction; Δg is the residual vector.

Here, the conjugate gradient algorithm is used to solve Equation (12) and to obtain the correction of the resistivity parameters of the subsurface cells.

2.3. Features and Benefits of ERT Technology

In addition to monitoring the dynamics of oil and gas reservoir development, ERT Technology plays an essential role in the oil and gas exploration process. Table 1 summarizes the current dynamic monitoring technology for oil and gas reservoir development. Compared with well logging technology, inter-well ERT has the following significant advantages: (1) high-resolution images: resistive tomography provides high-resolution stratigraphic images, which can meticulously reveal stratigraphic vulnerability, porosity, permeability, and other characteristics. (2) Real-time monitoring capability: resistivity tomography can monitor the resistivity changes of the formation in real-time, which can play a guiding role in drilling and oil and gas development. (3) Non-invasive measurement: electrical resistance tomography technology can reduce operational complexity and risk by measuring on the surface without underground operation. (4) Increased safety: Compared with traditional well logging technology [12,14], ERT technology is safer and more reliable in operation and can be widely used in various environments and scenarios [15,22]. (5) Based on big data analysis, electrical resistance tomography technology can use big data analysis methods for data processing and interpretation to improve the reliability and accuracy of data. (6) Unrestricted by geological complexity: electrical resistance tomography technology performs well in dealing with complex geological situations and can effectively reveal the inhomogeneity and heterogeneity of layers. (7) Simple and fast operation: Compared with traditional well logging technology, the operation of electrical resistance tomography technology is relatively easy and fast, which can save time and resource costs.

Table 1. Reservoir Dynamic Monitoring Technology has its advantages and disadvantages.

Reservoir Dynamic Monitoring Technology	Advantages of Methods	Limitation of Methods
Well logging technology	Radioactive well logging [43] <ul style="list-style-type: none"> • Deep penetration • Highly accurate • Integrity assessment 	<ul style="list-style-type: none"> • High safety risks • Restricted regulations • Complex data interpretation
	Acoustic logging g [44,45] <ul style="list-style-type: none"> • Wide logging scope • Accurate elastic parameter measurement 	<ul style="list-style-type: none"> • High wellbore requirements • Affected by mud • High-frequency attenuation
	Nuclear Magnetic Resonance (NMR) measurements [46,47] <ul style="list-style-type: none"> • Excellent fluid identification • Low invasion Effects 	<ul style="list-style-type: none"> • Expensive • Depth limitations
	Optical fiber logging [48,49] <ul style="list-style-type: none"> • Long monitoring time • High sensitivity 	<ul style="list-style-type: none"> • Original signal transmission distance limitation • Complicated installation and maintenance

Table 1. Cont.

Reservoir Dynamic Monitoring Technology	Advantages of Methods	Limitation of Methods
Production testing [50,51]	<ul style="list-style-type: none"> • Directly Assess Production capacity • Real-Time results • Support decision-making 	<ul style="list-style-type: none"> • Single Point Assessment • Production Interruption • Requires Multiple Testing
Well testing		
Transient testing [52,53]	<ul style="list-style-type: none"> • Dynamics around the pre-reaction wellbore • Mid-term acquisition of overall reservoir dynamics • Late stage to obtain clear reservoir shape 	<ul style="list-style-type: none"> • Limited time testing of middle and late-stage • Frequent interventions
Oil-Water sampling and analysis	<ul style="list-style-type: none"> • Oil-Gas quality assessment • Multi-parameter analysis 	<ul style="list-style-type: none"> • Interval limitations • Time and Cost
Tracer analysis method [54]	<ul style="list-style-type: none"> • Detects subtle fluid movement • Real-time monitoring 	<ul style="list-style-type: none"> • Environmental issues • Dependent on sampling points
Microseismic monitoring [55,56]	<ul style="list-style-type: none"> • Excellent reservoir characterization • Early warning of reservoir behavior 	<ul style="list-style-type: none"> • High equipment requirements • Limited geological conditions

3. Progress in the Application of ERT Technology

For the oil reservoir, natural gas reservoir, and coal mine in China, the ERT can be widely used to analyze residual oil distribution, capture flooding fronts, and monitor hydraulic fracturing. Section 3.1 of this section introduces the principles of ERT in the analysis of residual oil distribution in oilfields and then summarizes the application of ERT technology in the analysis of residual oil distribution in oilfields, emphasizing the important position of ERT technology in determining the recoverable reserves of residual oil, formulating the optimized oil recovery strategy, and improving the extraction efficiency of oilfields. In Section 3.2, some examples of the application of ERT in water drive front research are synthesized to help readers learn more about the application of ERT technology in monitoring water drive leading edge. Section 3.3 first describes the principles of ERT technology in hydraulic fracturing monitoring through textual descriptions and image displays, then summarizes the application of ERT technology in the process of hydraulic fracturing monitoring, and the application examples show the relevant researchers who have made use of ERT technology in the process of monitoring fractures. The overview of these examples can help readers better understand how ERT technology can help staff optimize hydraulic fracturing operations to ensure maximum extraction of oil and gas resources. Section 3.4 introduces some details about ERT devices and overviews some advances in ERT device optimization and algorithm improvement. In the past few years, ERT technology has seen widespread adoption across various oilfields, including those in Shengli, Daqing, and Changqing. With over 400 successful deployments and a remarkable 0% construction failure rate, detailed information can be found in Appendix A, Table A1.

3.1. Residual Oil Distribution Study

ERT technology can reveal the resistivity distribution characteristics of underground reservoirs and infer the location of the waterflood front edge and the distribution of residual oil. In general, underground reservoirs show non-uniformity, especially in the “favorable channel” with good porosity and permeability; the saturation of reinjected wastewater

is larger and the resistivity is relatively low, while the resistivity is relatively high in the lithologically dense section and the section with a large saturation of residual oil [57]. Anomalies in underground resistivity will have different effects on the distribution of surface potential values. Based on current-conductive theory in the uniform conductor [34–36], the distribution of the equipotential lines is a uniform concentric circle [40], as shown in Figure 3a. When one of the strata is replaced by high resistance, the surface equipotential line appears to be compressed inward (Figure 3b). When one of the strata is replaced by low resistance, the surface equipotential line appears to be extended to the place (Figure 3c).

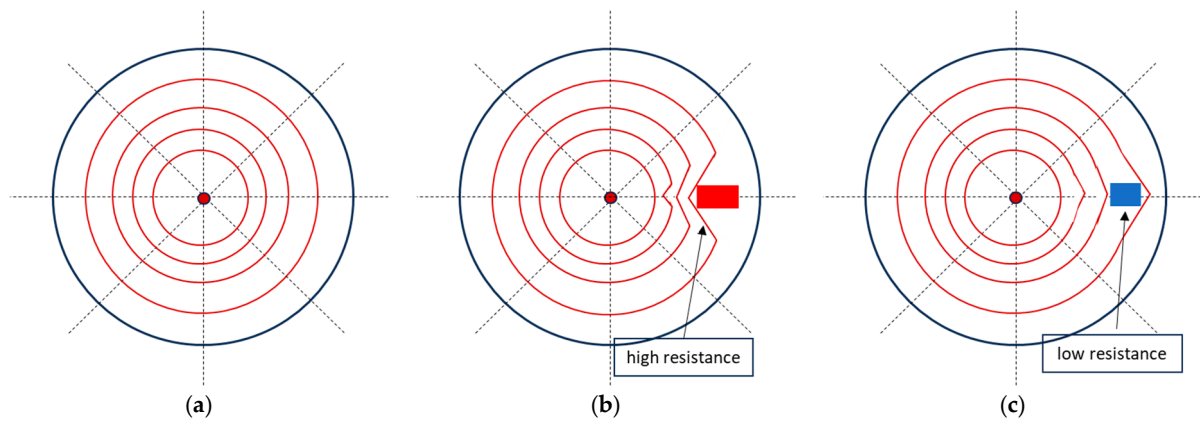


Figure 3. Top view of equipotential lines with different resistivities (a) Mean conductor equipotential line; (b) Presence of high resistivity equipotential line; (c) Presence of low resistivity equipotential line [58].

Therefore, combining the information of sedimentary phase distribution, lithology information, and formation water mineralization of underground strata, we use the anomalous potential inverse to perform the distribution image of resistivity and then calculate the distribution of oil saturation. For example, ref. [59], in response to the problem of unclear residual oil distribution in five wells of the Y Oilfield in the Muglad Basin, Sudan, and the unknown effect of water injection, used ERT to obtain the 3D resistivity distribution of the Aradeiba Formation in the basin (Figure 4). The high resistivity ($18\text{--}20\ \Omega\cdot\text{m}$) is distributed in the southeast of the top layer (Figure 4a) and the northwest, central, and southeast of the bottom layer (Figure 4b). The high resistivity is the high remaining oil saturation zone, and the low resistivity ($3\text{--}10\ \Omega\cdot\text{m}$) represents the high-water saturation zone. The black dots on the graph represent well locations. The difference in the resistivity distribution shows the oil saturation of the bottom layer is higher than the top layer as a whole, and Aradeiba has a strong heterogeneity and complicated oil-water interface.

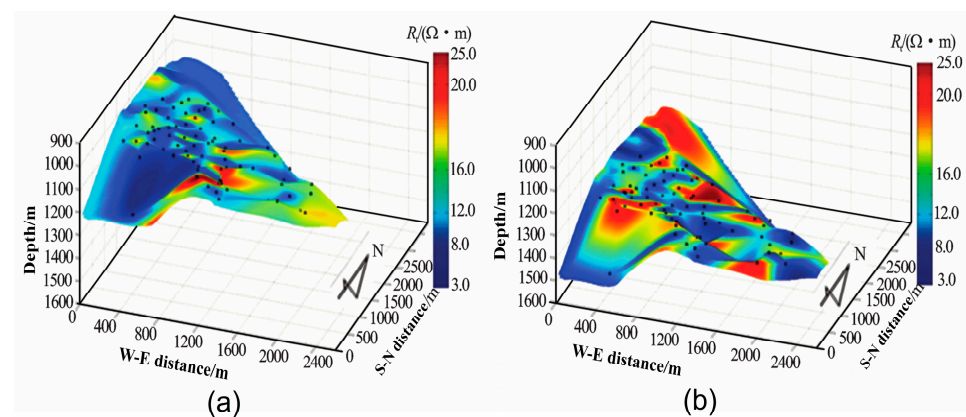


Figure 4. Three-dimensional resistivity distribution in the Aradeiba Formation: (a) top layer of the Aradeiba Formation; (b) bottom layer of the Aradeiba Formation [59]. Notes: The black points are the wellbore.

Then, their team used the resistivity slices obtained by inversion to calculate oil saturation slices, which revealed the block distribution of the remaining oil-rich area and the characteristics of the spatial distribution of oil and water [59]. Figure 5 shows the remaining oil saturation slices in the vertical direction from the upper to bottom depths. Since ERT measurement is achieved only by the tested wells in the objective formation, the image of the residual oil saturation distribution only covers the wells located in the tested formation. The white portion in the lower right of Figure 5 has many wells that are not in the tested formation. In the upper layer (Figure 5a), the remaining oil saturation in the northwestern zone (Y-82, Y-6, and Y-16) is relatively higher than the southeast zone (Y-24, Y-1, and Y-130), and the remaining oil saturation in the central region is as high as 70%, which is an obvious remaining oil collection area. In the middle layer (Figure 5b), the overall remaining oil is not high, and the remaining oil saturation in most areas is less than 50%. The bottom layer slice (Figure 5c) shows that the oil saturation enrichment area is the fault-block zone with about 70% remaining oil saturation.

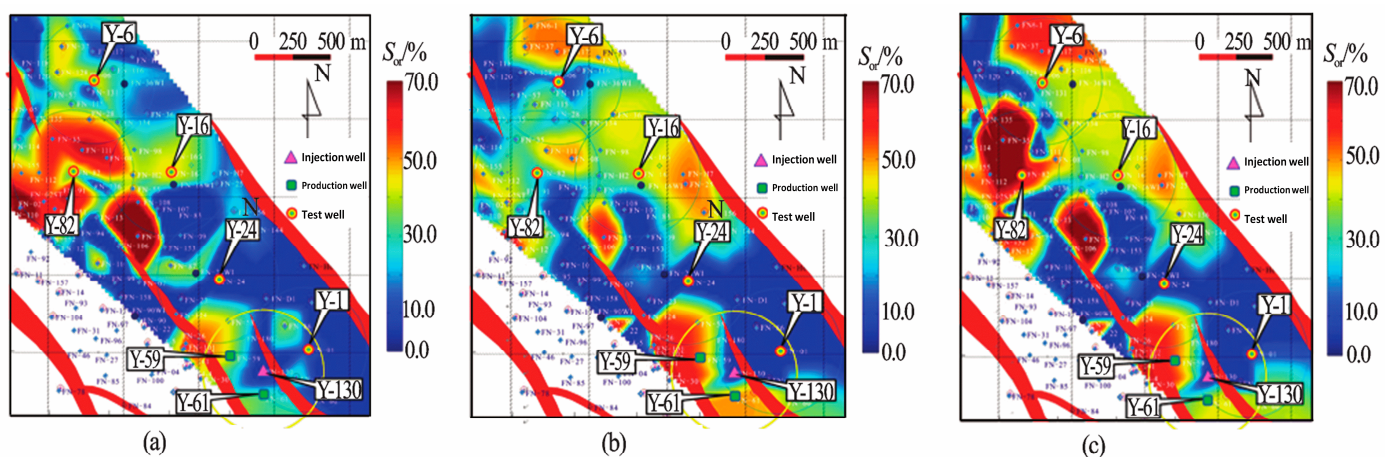


Figure 5. Oil Saturation Extended Layer Slices at the Bottom of Aradeiba (a) Slices located in the upper depth; (b) Slices located in the middle depth; (c) Slices located in the bottom depth [59] Note that the white zone is an untested formation.

Ref. [60] used ERT to obtain the field-measured potential data of the 26-J9 well zone of the eighth section in Gudong Oilfield, processed the measured potential data with numerical simulation and inverse imaging methods, and obtained the resistivity and residual oil saturation distribution of the target formation in the 26-J9 well zone. Ref. [61] focused on the application of the image processing method of well potential measurement data in the Wu1 Block of Xingjiang Oilfield and analyzed the correspondence between the distribution of residual oil and the effect of injection and extraction. Ref. [62] applied the ERT to measure and obtain the measured potential data of four blocks in the hilly reservoir, which provided a good basis for monitoring the residual oil distribution in a low-permeability sandstone reservoir. Ref. [63] focused on the residual oil distribution in the Daqing Oilfield based on the well-ground ERT technology. Ref. [64] established a three-dimensional geological model with ERT constraints by combining the resistivity and saturation distribution within the Chi-46 well area of JiYuan Oilfield with ERT technology and introduced reservoir evaluation parameters on this basis, which in turn led to favorable zone prediction of the reservoir. Ref. [65] focused on analyzing and evaluating the application effect of ERT technology in the Daqing Sabei Oilfield 9-102 well area, which showed the good application prospect of ERT technology in the remaining distribution study. Ref. [66] obtained more reliable ERT measurement data through EPI measurements and data processing of 7 wells in the Konys-406 well group in Area K, Kazakhstan, and the raw data truly and reliably reflected the resistivity of the subsurface. The resistivity and residual oil saturation distribution characteristics of the subsurface medium were obtained by inverse imaging of

the standardized potential data. Ref. [67] also verified the applicability of ERT technology in the target area by testing.

3.2. Waterflood Front Detection Study

Well-ground ERT technology can not only provide important clues about the formation characteristics and hydrocarbon distribution through the distribution of residual oil but also better evaluate the water drive effect and water injection program through the detection of the leading edge of waterflooding [68,69]. In the waterflooding process, due to the relative mobility difference between water and oil, the water pushes the oil toward the extraction well, forming the waterflood front. The purpose of the downhole ERT technology is to accurately monitor the change in subsurface resistivity, invert the resistivity distribution, and finally calculate the distribution of the waterflood front. For EOR in tight oilfields by the waterflood, the fracturing well is widely used in the injection-water well. To obtain the waterflood front information of the fractured injection-water well, [38] estimated the water breakthrough locations of multi-stage fractured horizontal wells by combining pressure-transient analysis and ERT. The injection well is the vertical well, and the production well is the horizontal well. Due to the fact that the wellbore of the production is longer than the injection-water well, the tested points are located at the production and distributed along the wellbore. Figure 6b is the calculated water flow front of the multi-stage fractured injection-water well in Figure 6a. The results show the waterflood fronts have just arrived at well B, and the water-breakthrough positions are located at the fourth and fifth perforations.

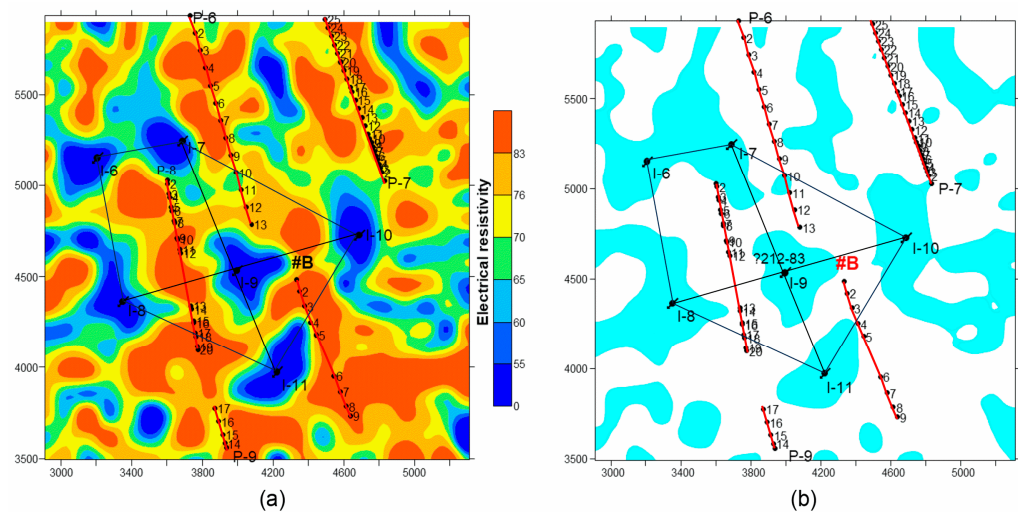


Figure 6. ERT results: (a) distribution of electrical resistivity; (b) waterflood front [38]. Notes: I-6, I-7, I-8, I-9, I-10, and I-11 are the injection-water wells. P-6, P-7, P-8, P-9, and #B are the horizontal production wells. The black points are the tested locations along the wellbore.

Ref. [70] tested the waterflood leading edge of the Zhuang 9 well area of the Xifeng oilfield by using the ERT technique and adopted the five-point method of well network injection to improve the water-driven effect in this type of reservoir. Ref. [71] inversely imaged the water injection and waterflood front in a muddy sandstone reservoir by placing electrodes in water injection and production wells using inter-well time-shift resistivity imaging. Ref. [72] monitored the results of brine tracers over time using well-ground and interwell electrical resistivity tomography. Based on the principle of well-ground ERT, the research team at China University of Geosciences (Beijing) established a multi-layer joint inversion method for large inclined and horizontal wells, inverted the ground potential response using the finite difference and conjugate gradient methods, and determined the transport direction of water bodies in each layer before and after injection by constructing 3D imaging maps of the injection layer [73].

3.3. Monitoring Dynamics of Hydraulic Fracturing Effects

Hydraulic fracturing is a process widely used in oil and gas exploration and development (Figure 7), based on the principle that fracturing fluids (mainly containing water, thickeners, sand, or other proppants) are injected into a well at high pressure, and the pressurized fluids pass through the well into the reservoir to fracture the rock. In this way, the fracture extends into the reservoir and increases the effective permeability of the reservoir, thereby increasing its ability to produce oil or natural gas.

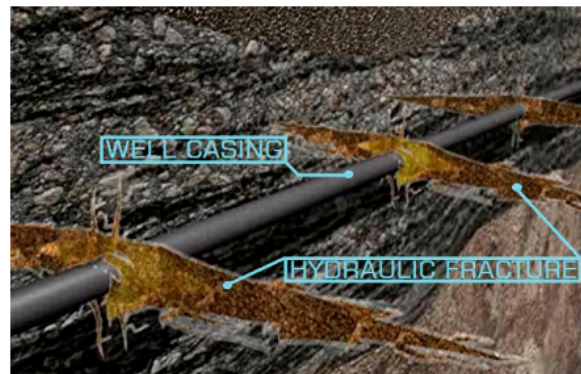


Figure 7. Fracturing fracture simulation [74].

Hydraulic fracturing has become a cost-effective and indispensable method for oil and gas exploration and development to modify the reservoir structure. In hydraulic fracturing, the orientation direction and real-time shape of the fracture are directly related to the effect of oil and gas reservoir modification; therefore, the real-time monitoring of fracture morphology is a key technology in the fracturing process, and the ability to accurately monitor the fracture orientation and geometric parameters directly affects all aspects of evaluating the fracturing effect, improving the fracturing process, and improving the recovery rate of oil and gas [74]. The application principle of ERT technology in the hydraulic fracturing process is to use the casing and fractured fractures filled with conductive fracturing fluid as the transmission medium to inject high current into the subsurface to form a subsurface electric field, and then to deploy ring-shaped measuring electrodes at the wellhead of the measuring wells located on the surface, and to use the measured potential data to invert and derive the information of the relevant parameters of the subsurface fractures as shown in Figure 8.

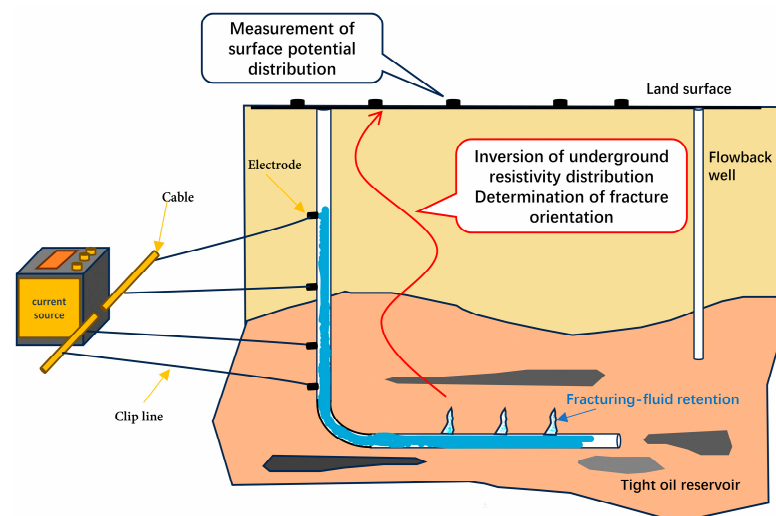


Figure 8. A schematic diagram of the application of ERT technology in the hydraulic fracturing process.

The determination of artificial fracture azimuth and fracture extension length is the main problem of the wellbore potentiometric method in hydraulic fracturing, and many researchers have conducted extensive research on this issue. The Institute of Enhance Oil Recovery Technology of Dagang Oilfield, China, has researched monitoring fracture azimuth using a well-ground potentiometric method since the 1980s and initially formed a series of more mature potentiometric monitoring technology systems.

Ref. [75] obtained the geometric parameters of fracture distribution before and after hydraulic fracturing of the M1 well in the coalbed methane exploration area of the Beipiao coal mine by using ERT technology, which demonstrated that ERT technology has a good prospect of application for detecting hydraulically fractured joints. Ref. [76] introduced the potentiometric well monitoring technique for the real-time detection of fracture size and orientation during the fracturing process to deploy the whole well network for the development of extra-low permeability reservoirs in the Wuhaozhuang reservoir of Shengli Oilfield and judged the fracture location by the outer ring potentiometric anomaly curves, which provided the theoretical basis for the deployment of the well network in the subsequent blocks and the analysis of the fracturing effect.

In addition, Ref. [77] analyzed and evaluated the hydraulic fracturing process of Carboniferous volcanic reservoirs in the J230 well area of Karamay Oilfield by using ERT fracture monitoring technology for data monitoring, which provides a reference basis for the optimal design of fracturing in this type of reservoir, the preferred selection of action scheme, the overall treatment of injection and extraction units, and the improvement of recovery rate. Ref. [78] conducted indoor and outdoor experiments, respectively. The outdoor experiments took Chao 121-27 in the Chaoyanggou oilfield of Daqing 10th plant as the research object, and the fracture orientation was inferred by the potential anomaly curve (shown in Figure 9), which laid the foundation for the start of ERT technology fracture monitoring field experiments.

Ref. [79] conducted the research on the hydraulic fracturing dynamic monitoring method based on wellbore ERT technology and used finite element COMSOL software (<https://cn.comsol.com/>) to successively optimize the current source model, and the results of its inverse performance were more consistent with the actual morphology of the fracture. They then verified the correctness of the orthogonal model through flume simulation experiments. Ref. [80] used the new ERT method to successfully estimate the range and aperture diameter of hydraulic fracturing, which provided the basis for oil and gas recovery and thermal engineering support. Ref. [81] considered that a complex fracture network providing flow channels would have a significant impact on well performance in unconventional reservoirs. A foundation was laid for subsequently obtaining more accurate rate transient responses as well as fracturing parameter estimation. The team from China University of Petroleum (Beijing) adopted a multi-section fractured horizontal fluid production profile monitoring method for multi-fractured horizontal wells (MFHWs) in Changqing Oilfield by combining the unstable well test and well ground ERT techniques and effectively diagnosing the location of water seen in the wellbore of MFHWs [38,81,82]. Their team also studied fractures induced by water drives around injectors in tight reservoirs. By studying fracture length, fracture conductivity, bottom-hole pressure [83] and other related parameters, a new semi-analytical model is proposed. The new progress of water injection-induced dynamic fracture characterization technology at home and abroad is clarified, and the impact of dynamic fracture on water injection development and the well network encryption adjustment strategy based on dynamic fracture are systematically elaborated [84]. In addition, the research team introduced big data technology applied to the prediction of reservoir parameters and evaluation of well production capacity in oil fields in the western part of the South China Sea [85].

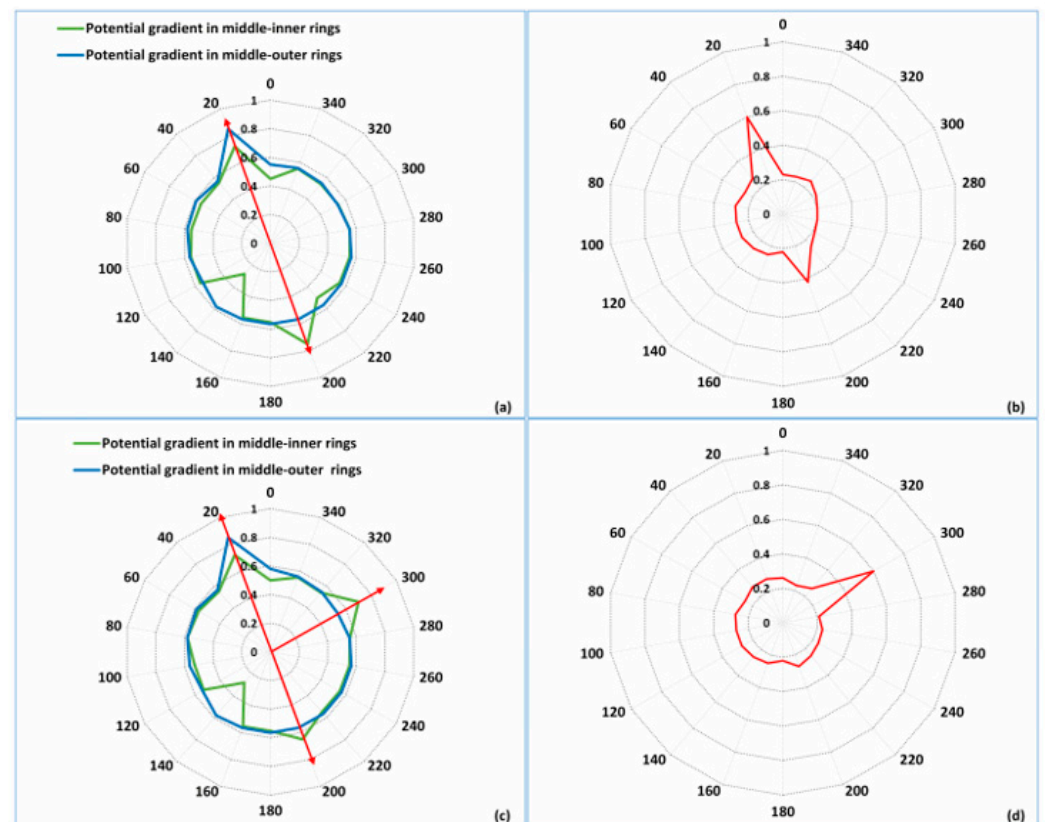


Figure 9. Potential anomaly curve extrapolates the crack orientation map: (a) Radar map of purely anomalous curves after deep fracturing; (b) Inferred deep fracture orientation map; (c) Radar map of purely anomalous curves of fractures after fracturing in two layers; (d) Inferred orientation of fractures in shallow layers [78].

Ref. [86] studied the orthogonal model, numerical simulation, and optimized design of the on-site monitoring system and data analysis of the well-ground potential measurement method, and further verified the reasonableness of the orientation and length prediction of fractured fractures using the potential method by using the finite element COMSOL software, which will be a reference value for the future improvement of fracturing operation effects and optimization of fracturing design.

3.4. Advances in Well-Ground ERT Equipment Improvement and Forward and Backward Optimizations

Equipment optimization and algorithm optimization are the key driving factors to promote the continuous development and application of well-ground ERT technology and are also important ways to realize the efficient cooperation and optimized performance of the various parts of the well-ground ERT workflow. Specifically, the well-ground ERT work operation is mainly composed of the surface multi-electrode array, power source, data acquisition and processing unit, and image reconstruction and analysis unit. As shown in Figure 10, a multiple-line electrode array is used in the horizontal wellbore to measure the resistance of the reservoir during the injection and production testing processes. In the test process, the equipment and the inverse algorithms play a very important role. Therefore, the advanced equipment and optimized forward and inverse algorithms promote each other to improve the accuracy and efficiency of data acquisition and optimize the accuracy and reliability of image reconstruction and parameter inversion.

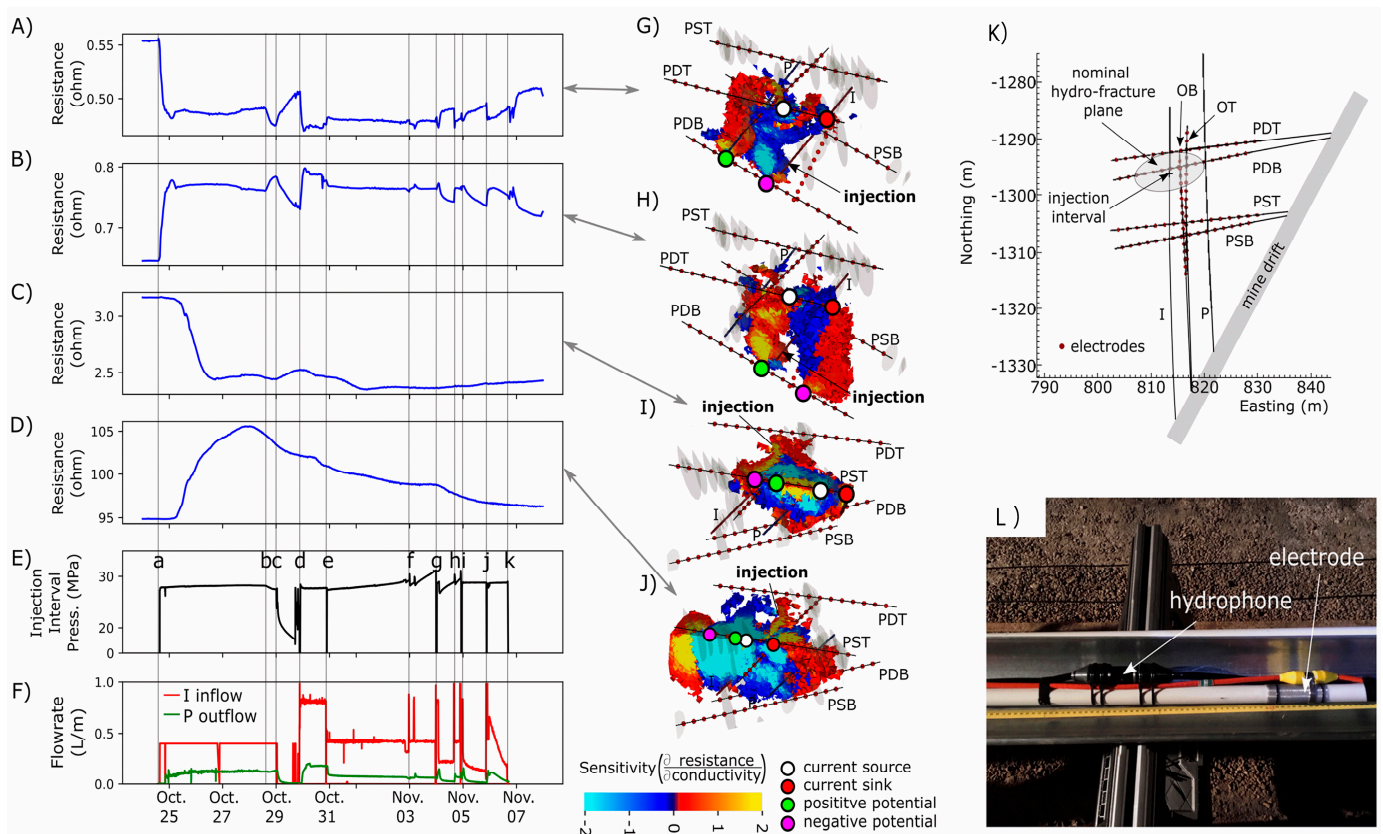


Figure 10. (A–D) example electrical resistivity tomography data time series with respect to (E) Injection interval pressure with stop time of pump (a–k) and (F) Injection and production flow rate. The time series in panels (A–D) corresponds to the electrode positions in panels (G–J). Vertical lines are provided as an aid to align the times of notable events between plots. (G–J) Sensitivity distribution of the change in observed transfer resistance with respect to the change in bulk electrical conductivity (BEC) for measurements (A–D), respectively an increase in BEC within a region of positive sensitivity (warm colors) will cause an increase in transfer resistance, and vice versa. Note that the injection intervals in (I, J) are obscured by the sensitivity map. (K) Plan view of injection (I), production (P), and monitoring borehole (OB, OT, PDT, PDB, PST, and PSB) orientations. Each borehole originates at the drift wall and terminates as shown. (L) Photograph of monitoring borehole instrumentation string prior to installation. Each instrumentation string was grouted in place prior to stimulation [87].

3.4.1. Equipment Optimization

Equipment optimization aims to improve measurement efficiency and data quality so that the borehole ERT can obtain the underground resistivity distribution information faster and more accurately by improving the electrode design and placement, optimizing the data acquisition instrument, improving the multi-electrode array design, and introducing system control and automation technology. Figure 11 shows the four common electrodes widely used in the oilfield, which belong to the new non-polarized electrodes. Many oilfield test results [88] show that this type of electrode has a good receiving signal effect. This type of testing accuracy has been increased from the millivolt to the micro-level, and it is more authentic and effective to collect information on the ground electric field, which greatly improves the credibility of observation data.



Figure 11. ERT non-polarized electrode types: (a) Oilfield electrode; (b) Ukrainian electrode; (c) Trial electrode; (d) Copper rod electrode [88].

At present, research scholars in the U.K. have conducted many studies on equipment improvement and algorithm optimization. Aiming at different engineering backgrounds of oil-gas-water multiphase pipe flow generation, Mi Wang's research team at the University of Leeds, UK, has successively designed various electrode sensor arrays such as annular [89], linear, parallel, and U-shaped [90], developed single/dual/multi-sectional unimodal and double-modal inspection devices, and established supporting image reconstruction algorithms, and established supporting image reconstruction algorithms, and applied the double-model electrostatic tomography (ERT-ECT) technique to identify the stratified flow (Figure 12a), slug flow (Figure 12b), plug flow (Figure 12c), annular flow (Figure 12d), and bubbly flow (Figure 12e) within the oil-gas-water three-phase flow system in a horizontal pipe [91–93]. Usually, ERTs recognition of non-liquid phases, especially gas, is not very good; however, in Mi's double-model, the gas (red in Figure 11), oil (yellow and green in Figure 11), and water (blue in Figure 11) are very easily captured and calculated by the ERT field. The results show that the improvement and upgrade of ERT equipment is an important way to accurately obtain fluid parameters.

Ref. [88] has developed high-quality unpolarized electrodes with small differential potentials, good stability performance, low noise, wide bandwidth, light and durability, and easy storage in response to the disadvantages of well-ground ERT electrodes, which are similarly affected by the natural potentials of the well and ground sites and the interference of industrial frequency, the change of ambient temperature, and the polarization phenomenon of electrodes. More accurate data processing of the measured data will further provide effective technical support for the development and utilization of petroleum and minerals. In addition, Ref. [94] improved the well-ground ERT equipment and designed a synchronization scheme combining Beidou satellite timing technology, a local clock system, and wireless radio frequency transmission technology, which was applied to the well-ground water-driven leading edge and fractured fracture resistivity stratigraphic imager, so that the data collected by the instrument in the test were guaranteed and reached the synchronization level of the similar geological exploration instruments at home and abroad. Ref. [95] investigated the ERT data quality control problem, proposed a bipolar-bipolar co-current channel set method for rapid detection of ERT data quality, and suggested data quality control and hydraulic conductivity fracture delineation before ERT inversion and tracer testing. Ref. [96] focused on small-scale ERT for high-resolution subsurface imaging,

including 3D modeling and electrode configuration. It was deduced that small-scale ERT requires accurate electrode representation and placement. Ref. [97] designed a hybrid resistivity tomography and induced polarization (ERT/IP) cable/distributed system. This system with multi-source capability allows for the transmission of as many sources as possible when using separate lines, thereby increasing the current input to the ground and increasing the depth of investigation and resolution. To develop an inter-well ERT system for CO₂ transport monitoring in the formation, Ref. [98] optimized the electrode array and verified its usability.

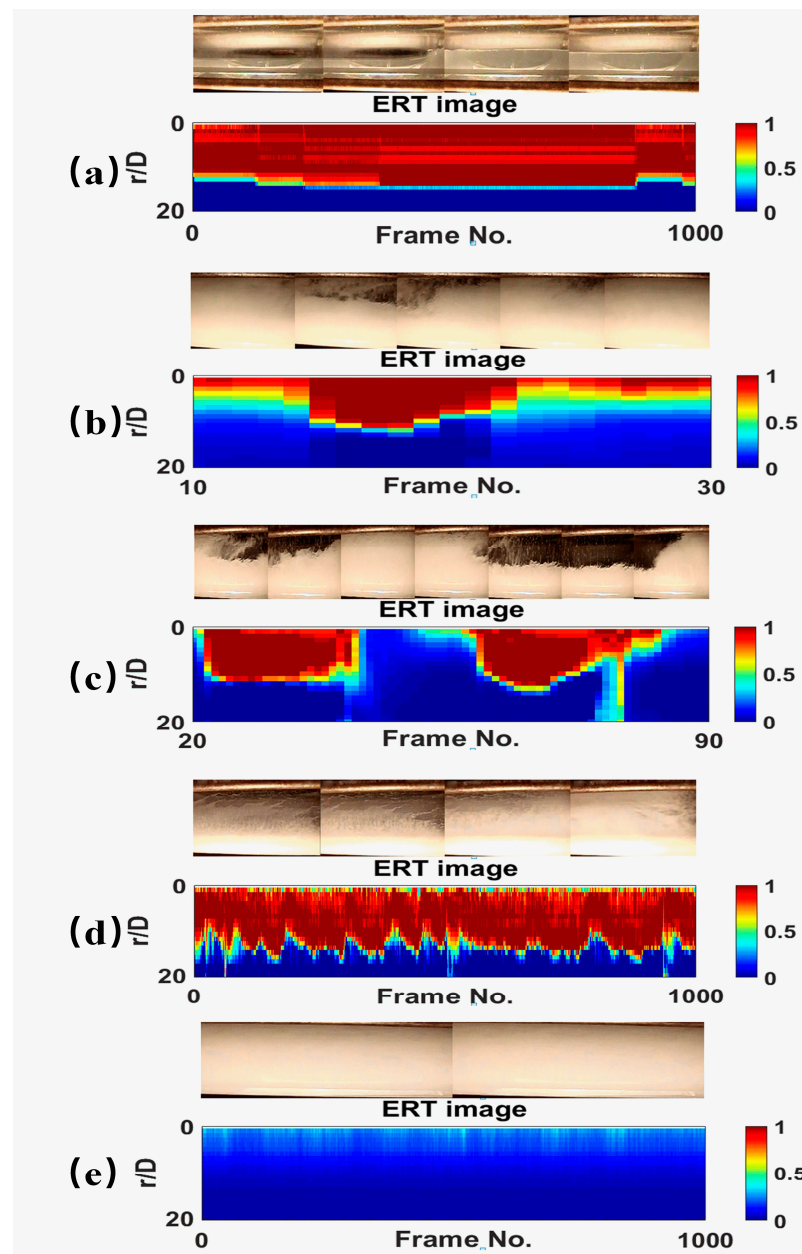


Figure 12. Visualization results for five types of flow (a) stratified flow; (b) slug flow; (c) plug flow; (d) annular flow; and (e) bubbly flow [90].

3.4.2. Algorithm Optimization

Algorithm optimization focuses on improving data processing and interpretation capabilities. By improving the data processing and inversion algorithms, the Well-Ground ERT technique can more accurately reconstruct subsurface structure and properties from measured data. Optimized data processing algorithms filter out noise, correct data, and

provide more accurate interpretations. Improved inversion algorithms provide engineers with more detailed information about subsurface structure by more accurately inverting the resistivity distribution of the subsurface medium from resistivity measurements. To study the surface potential response caused by 3D anomalies in the subsurface, [99] designed an orthogonal algorithm of a well-ground ERT technique based on practical problems and finally gave the map obtained by the orthogonal algorithm. The constraints are provided, and the foundation is laid for further 3D inversion studies. Ref. [100] investigated point current sources (single or multiple points) and arbitrary line current sources when supplied in a well and three-dimensional resistivity forward and inverse under the ground receiving mode. It provides a very meaningful guide for the design of field observation systems. [101] discussed the method of underground vertical line source segmentation calculation and field superposition and realized the 3D numerical simulation of DC power supply on the casing, which provides some reference basis for the design of the well-ground ERT technology. Ref. [102] investigated an intrusive resistive tomographic imaging sensor for vertical oil well production logging, applying a sensitivity-based algorithm for image reconstruction. Ref. [103] completed Bayesian ERT inversion based on non-smooth inverse martensitic covariance matrices. A team of researchers led by the Pacific Northwest Laboratory (PNNL) in the United States intentionally measured electrical conductivity in rocks using the ERT program and generated 4D (3D + time-lapse) images of the subsurface. In addition, Tim Johnson, a key member of the team, has developed E4D software (<https://www.pnnl.gov/projects/e4d>, accessed on 15 August 2023) that runs on a supercomputer and displays all the electrical signals and fluctuating conditions over time in a heat map-like visualization [87].

Ref. [104] studied the problem of three-dimensional resistivity inversion polysolvability and proposed a method based on the constraints of the reference model. By fusing multiple geophysical information, an accurate reflection of anomaly morphology and resistivity is achieved, and polysolvability is suppressed. Ref. [105] investigated the resistivity logging problem in the two-phase test wells of water injection, and using iterative numerical algorithms and orthogonal simulation methods, they concluded that the resistivity logging data can reflect the change in water mineralization. Ref. [106] used the DBSCAN (Density-Based Spatial Clustering of Applications with Noise) clustering algorithm to improve the interpretation of the inverted ERT sections.

4. Conclusions and Future Prospects

Electrical Resistivity Tomography (ERT) plays an important role in oil and gas reservoir monitoring. By measuring the resistivity distribution of subsurface reservoirs, ERT provides valuable information for the development and management of oil and gas reservoirs. With its high-resolution and non-invasive characteristics, ERT can provide quantitative data support to help optimize the oil recovery scheme, evaluate the remaining resources in the reservoir, and provide scheme support for adjusting the production work system to improve the oil and gas recovery rate. At present, the development trend and future research direction of ERT technology in the field of oil and gas reservoir monitoring can be summarized in the following aspects:

- (1) Overall exploration of the oil and gas reservoir field, searching for residual oil-rich areas and sweet spots of hydrocarbons. Based on the development well network structure of the oil and gas field, some wells are selected as current injection wells, and the remaining wells are used as current return wells, with the entire reservoir as well as the internal fluid as the current flow medium. By arranging the sensor matrix on the surface to obtain the voltage signal, the inversion obtains the underground reservoir and fluid information, especially the distribution location of the remaining oil in the reservoir. This ERT method has been better applied in Daqing Gudong, Sabei Oilfield, Karamay Oilfield, and Changqing Jiyuan Oilfield in China.
- (2) Monitoring the dynamics of the development process. Waterflooding development process: real-time access to waterflooding dynamics is an important part of the devel-

opment process and is the basis for implementing the improvement and adjustment of the replacement program. In the field, some well networks are used as power injection-return lines, and the resistivity field maps of the blocks are mostly obtained by inversion of linear sensor matrix data, thus determining the oil-water distribution boundary or the location of the waterflooding leading edge. This ERT method has been well applied in Changqing Wuqi, Xifeng Oilfield, and Daqing Lamaideen Oilfield in China.

- (3) Monitoring dynamics of reservoir physical properties and fluids around injection-production wells during the full production life cycle. In the field, the injection and extraction well group is used as the current injection-return line, and most of the radiation sensor matrix data are used to invert the fracture extension dynamics, fracture development orientation, water injection, and water absorption profiles around the wells. This ERT method has been successfully applied in the Yanchang Zichang Oilfield, Shengli Wuhaozhuang Oilfield, Karamay Oilfield, Daqing Chaoyangguo Oilfield, and Beipiao Coal Mine Coalbed in China.
- (4) The future direction of well-ground ERT development and optimization remains optimization of inversion algorithms and optimization of monitoring equipment. The current research status of the inversion algorithm is mostly the full-space, multi-scale inversion method, which utilizes all and multi-scale observation data to improve the resolution, stability, and adaptability of the inversion results under some specific geological conditions. In addition, ERT inversion is mostly combined with methods such as deep learning and neural networks to improve imaging results. The optimization of the ERT inversion technique has yielded good results, and there are directions for future improvement: (i) The ERT inversion problem is usually multiplicity, and there may be multiple subsurface models that match the measured data; therefore, how to enhance the uniqueness of the inversion results remains an important issue for future research. (ii) Optimize the algorithm to improve the inversion speed and computational efficiency. (iii) Consider nonlinear and complex media.
- (5) Currently, researchers are focusing on optimizing the electrode arrangement, using highly conductive electrode materials, and developing more advanced data acquisition and processing systems to achieve faster and more accurate data acquisition and real-time data processing. Future improvement directions include: (i) Multiple frequency measurement, using multi-frequency current injection for dealing with complex media and multi-layer underground structures. (ii) Adaptive electrode configuration, which automatically adjusts the electrode arrangement according to the actual site conditions and exploration targets to improve data utilization efficiency and imaging accuracy.

Author Contributions: Conceptualization, W.S., and M.W. (Mi Wang); methodology, W.S.; software, G.Y.; investigation, G.Y., and W.S.; resources, L.T.; data curation, J.B., and Z.X.; writing—original draft preparation, G.Y., and W.S.; writing—review and editing, M.W. (Mi Wang); visualization, M.W. (Mengjun Wu) and Z.Y.; supervision, Q.Z., and L.T.; project administration, W.S.; funding acquisition, W.S. All authors have read and agreed to the published version of the manuscript.

Funding: This research was funded by the “Chunhui Plan” of the Ministry of Education (China) (No. HZKY20220144), the Fourth Batch of Leading Innovative Talent’s Introduction and Cultivation Projects of Changzhou (No. CQ2022012), and the Research Funding Projects of Changzhou University (No. ZMF22020071).

Data Availability Statement: Not applicable.

Acknowledgments: The authors would like to thank Liu Li, Analysis and Testing Center, NERC Biomass, Changzhou University.

Conflicts of Interest: The authors declare that they have no known competing financial interest or personal relationships that could have appeared to influence the work reported in this paper.

Appendix A

Table A1. Application of ERT in oil and gas reservoirs and coal mines in the past 20 years.

Year	Oilfield Co.,	Oilfield/ Mine	Block/Well	Reservoir Type	Test Projection and Objection	Current Loop	Surface Sensor Matrix	Current Intensity
2021	Sanford Underground Research Facility (SURF)	/	Foorman formation	Tight reservoir: $\varphi < 1\%$	remote monitoring of stress-induced pore size distribution changes during high-pressure injection in tight fractured rock systems at tens of meters scale using time-lapse 3D resistivity tomography [87]	horizontal well group	Upper cross grid with 2 lines in W-E (PDT, PST) and 1 line in N-S (OT), bottom cross grid with 2 lines in W-E (PDB, PSB) and 1 line in N-S (OB)	/
2020	Changqing	Huaqing	Bai121 block, Yuan 427 block	middle-porosity low-permeability sandstone reservoir: $\varphi = 16\%$, $k = 15$ mD	effect of injection water and the distribution of oil and water	well group with 2.0 km	radial: $20^\circ \times 50$ m	15~20 A
2020	Jingcheng mine	/	CS-01well3-	/	shape, direction, and length of fracture in the fracturing process	/	/	/
2020	Changqing	/	/	low-permeability reservoir: $\varphi = 10.6\%$, $k = 1.0$ mD	flowrate of fracture and breakout location of the water body [38]	well group with 1.5 km	radial: $20^\circ \times 50$ m \times 30 rings	/
2020	Sudan	Y	Y-130 well	anticline fault block reservoirs: $\varphi = 20\%$	oil distribution of every profile and section [59]	/	radial: $15^\circ \times 25$ m \times 16 rings (25~400 m)	/
2019	Changqing	/	X90-5 fractured well	tight reservoir: $\varphi = 12.69\%$, $k = 1.81$ mD	injection-production connectivity, flow velocity [82]	/	/	/
2019	Changqing	/	Liu X block	/	remaining oil distribution, waterflooding front, fractures, shape, and distribution	well group with 0.8 km	/	/
2018	Sudan	X	5 wells	sedimentary sandstone and mudstone	evaluation of remaining oil distribution	/	radial: $15^\circ \times 25$ m \times 16 rings (from 25 m to 400 m)	/

Table A1. Cont.

Year	Oilfield Co.,	Oilfield/ Mine	Block/Well	Reservoir Type	Test Projection and Objection	Current Loop	Surface Sensor Matrix	Current Intensity
2017	Yanchang	Zichang	Anding Block	Chang6 oil formation	change in distribution and shape of fractures in the fracture process	/	/	/
2015	Daqing	Lamadi	North block (9 wells)	sandstone	residual oil, injection water progress			
2015	Daqing, Shanxi coal mine	Chaoyanggou, Yanchun- nan	Chao75-149 well, Yan6-20-26 well	/	Change of shape and angle of fracture	injection well vs. another well at a distance of 1.5–2.0 times the test depth	radial:20° × 50 m × 3 rings (50 m–100 m–150 m)	50 A
2014	KAM of Kazakhstan	Konys	konys-406 block (7 wells)	sandstone	distribution of remaining oil in each layer of the 12 planes, water injection propulsion, and sweeping range [66]	well group with 1.8 km	15° × 25 m × 12 rings (from 25 m to 300 m)	/
2013	Changqing	Xifeng	Zhuang 9 Block	/	water flooding front, well pattern water injection effect evaluation [70]	/	/	/
2013	Daqing	Chaoyanggou	/	/	fracture orientation was deduced from the potential anomaly curve [78]	/	/	/
2012	Changqing	Jiyuan	Chi46 well	/	distribution of the remaining oil [64]	/	/	/
2012	Daqing	Sabei	9-102 block	/	distribution of the remaining oil in the main layer	well group with 1.0 km	radial: 20° × 50 m × 8 rings	/
2012	Xinjiang	Karamay	J230 Block	/	capture the change process of the fracturing [77]	/	/	/
2012	Xinjiang	Karamay	J230 Block (951738 well, Bai905 well)	low-porosity low-permeability fractured reservoir	analysis and evaluation of fracturing and refracturing effects, fracture occurrence, etc.	injection well vs. another well at very far	radial:15° × 20 m × 3 rings (30 m–50 m–70 m)	20 A

Table A1. Cont.

Year	Oilfield Co.,	Oilfield/ Mine	Block/Well	Reservoir Type	Test Projection and Objection	Current Loop	Surface Sensor Matrix	Current Intensity
2011	Changqing	Wuqi	Wu410 block	/	capture the water injection propulsion front and ascertain the propulsion direction and sweeping range of the injected water.	/	/	
2011	Shengli	Wuhaozhuang	/	/	judging the position of the crack by the abnormal curve of the outer ring potential	/	/	/
2011	Shengli	Wuhaozhuang	Zhuang74 block, Zhuang59 block	low-porosity low-permeability high-temperature high-pressure reservoir: $\phi = 16.4\%$, $k = 19$ mD	real-time detection of fracture size and orientation during fracturing [76]	injection vs. production well group	$15^\circ \times 30$ m \times 3 rings (70 m–90 m–100 m)	/
2010	Changqing	Suijing	Yang42 block	/	shallow reservoir evaluation	/		/
2009	Daqing	Xingshugang, Lamadian, Longhupao	Nan4 block(2 wells), Xiang1 block(4 wells), 8 and 9 block(9 wells), center block (2 wells)	$\phi = 15.3\%$, $k = 0.51$ mD	blockage after polymer injection, water channel, connectivity judgment, water channel, distribution of remaining oil [63]	well group with 1.0 km	$20^\circ \times 50$ m \times 8 rings	/
2009	Changqing	/	H1~H6 well	/	identify fracture orientation, shape, symmetry, and other parameters	/	$15^\circ \times 20$ m \times 3 rings (60 m–80 m–100 m)	20 A
2009	Changqing	Ansai	9 block (11 wells)	low-porosity low-permeability reservoir	remaining oil distribution, reservoir prediction	well group with 2.0 km	$20^\circ \times 50$ m \times 18 rings	/
2008	Xinjiang	Karamay	si2 block	heavy oil reservoir: $\phi = 18.8\%$, $k = 8.2$ mD	steam water drive channel, research on remaining oil distribution	/	/	

Table A1. Cont.

Year	Oilfield Co.,	Oilfield/ Mine	Block/Well	Reservoir Type	Test Projection and Objection	Current Loop	Surface Sensor Matrix	Current Intensity
2008	Tuha	Quling	Ling4 block (5 wells)	low-porosity low-permeability: $\varphi = 13.8\%$, $k = 14.1$ mD	sand body distribution, water flooding profile, remaining oil between wells, main water flow direction of small layers	well group with 1.2 km	radial: $20^\circ \times 50$ m \times 8 rings	/
2008	Changqing	Ansai	Yanghewan25 block (9 wells)	low-porosity low- permeability: $\varphi = 9.89\%$, $k = 0.308$ mD	study on prediction of favorable areas of reservoir	well group with 2.0 km	radial: $20^\circ \times 50$ m \times 30 rings	/
2008	He'nan	Shuanghe	Center block (5 wells)	/	water injection channel, seepage channel, remaining oil distribution	well group with 1.2 km	radial: $20^\circ \times 50$ m \times 9 rings	/
2006	coal mine	Beipiao	M1 well	/	geometric parameters of fracture distribution before and after fracturing [75]	well group with 1.1 km	$20^\circ \times 50$ m \times 9 rings	10 A
2006	Daqing	Sabei	3 block (2 wells)	/	distribution of remaining oil and water channeling during injection [65]	/	/	/
2005	Xinjiang	Karamay	Wu1 block	/	correspondence relationship between remaining oil distribution and injection-production effect, four-dimensional oil-water dynamic analysis [61]	well group with 1.5 km	/	/
2004	Shengli	Gudong	8 Block (26-J9 and 26-2008)	sandstone	polymer flooding effect of well 26-j9 and remaining oil distribution after polymer injection [60]	well group with 1.5 km	radial	/

Table A1. Cont.

Year	Oilfield Co.,	Oilfield/ Mine	Block/Well	Reservoir Type	Test Projection and Objection	Current Loop	Surface Sensor Matrix	Current Intensity
2002	Shengyang	Shenyang	An1-An97 block and Biantai block (6 wells includes Sheng21-12)	ancient, buried hill fractured reservoir: $\varphi = 7.5\sim 12\%$	find out the direction of water injection and flooding, study the development direction of micro-fractures, balance the contradiction between injection and production, and rationally adjust the development plan. [60]	Sheng 31-12 vs. Sheng 21-13	radial: $15^\circ \times 100 \text{ m} \times 2 \text{ rings};$ (70-170 m)	/

References

1. Femi, F.A. Mapping a Spatial Salinity Flow From Seawater to Groundwater Using Electrical Resistivity Tomography Techniques. *Sci. Afr.* **2021**, *13*, e00957.
2. CiaCiampi, P.; Esposito, C.; Cassiani, G.; Deidda, G.P.; Flores-Orozco, A.; Rizzetto, P.; Chiappa, A.; Bernabei, M.; Gardon, A.; Petrangeli Papini, M. Contamination Presence and Dynamics at A Polluted Site: Spatial Analysis of Integrated Data and Joint Conceptual Modeling Approach. *J. Contam. Hydrol.* **2022**, *248*, 104026. [[CrossRef](#)] [[PubMed](#)]
3. Kondracka, M.; Stan, I.; Sitek, S.; Ignatiuk, D. Evaluation of Geophysical Methods for Characterizing Industrial and Municipal Waste Dumps. *Waste Manag.* **2021**, *125*, 27–39. [[CrossRef](#)]
4. Xiujun, G. A Study of Detecting Contaminated Soil Layers and Aquifers Using Resistivity Tomography Method. Master's Thesis, Ocean University of China, Qingdao, China, 2009.
5. Ling, C.; Zhou, Q.; Xue, Y.; Zhang, Y.; Li, R.; Liu, J. Process Analysis of Water Migration in Anaerobic Landfill Column Based on ERT. *Acta Sci. Circumstantiae* **2012**, *32*, 1942–1951.
6. Dong, L.; Ye, T.F.; Nai, C.X.; Liu, Y.Q.; Gong, Y.L.; Chen, Y. Application of ERT Technology to Investigate Inorganic Polluted Site. *Res. Environ. Sci.* **2008**, *21*, 67–71.
7. Zhang, T.; Zhang, W.R.; Liu, X.C.; Xu, C.H.; Liu, R.G. Research progresses of principle and application of biomedical magnetic induction tomography. *Chin. Med. Equip. J.* **2022**, *43*, 81–87. [[CrossRef](#)]
8. Shi, X.; Wang, L.; Xu, H.; Xu, Q.; Cao, S.; Xu, M. Quantitative characterization of decay detection in standing trees of Korean pine based on Resistograph and ERT. *J. Beijing For. Univ.* **2017**, *39*, 102–111.
9. Li, Y.L.; Sun, H.L.; Liu, C.L.; Xing, L.C.; Wu, N.Y.; Meng, Q.G. Application of ERT to Hydrate Monitoring: Take Ice as Substitute. *Mar. Geol. Front.* **2020**, *36*, 65–71.
10. Wang, P.; Liu, Z.; Jia, B.; Liu, L. 3D visual detection method of mine filling pipeline blockage based on ERT technology. *J. China Coal Soc.* **2023**, *48*, 2465–2474.
11. Wang, J.; Wu, A.; Wang, M.; Ruan, Z. Experimental Investigation on Flow Behavior of Paste Slurry Transported by Gravity in Vertical Pipes. *Processes* **2022**, *10*, 1696. [[CrossRef](#)]
12. Ma, Y.X.; Xu, L.A.; Jiang, C.Z.; Shao, J.Q. Study of Electrical Resistance Tomography. *Chin. J. Sci. Instrum.* **2001**, *630*, 195–198.
13. Wang, H.X.; Wang, J.; Hu, L.; Jiang, W.W.; Hao, K.H.; Song, Z.J. Optimal Design of ERT/ECT Dual-Modality Sensing Electrode Array. *J. Tianjin Univ.* **2008**, *8*, 911–918.
14. Ye, Z.; Wei, H.Y.; Soleimani, M. Resolution Analysis Using Fully 3D Electrical Capacitive Tomography. *Measurement* **2015**, *61*, 270–279. [[CrossRef](#)]
15. Garde, H.; Hyvonen, N.; Kuutela, T. On Regularity of the Logarithmic Forward Map of Electrical Impedance Tomography. *Siam. J. Math. Anal.* **2020**, *52*, 197–200. [[CrossRef](#)]
16. Sharma, S.K.; Khambampati, A.K.; Kim, K.Y. Estimating Aquifer Location Using Deep Neural Network with Electrical Impedance Tomography. *J. IKEEE* **2020**, *24*, 982.
17. Onwa, N.M.; Ikenna, A.O. Application of the 2D Electromagnetic Tomography in Delineating Groundwater Zones in Pre-Santonian Fractured Sedimentary Rocks in Abakaliki Area, Southern Benue Trough, Nigeria. *Arab. J. Geosc.* **2022**, *15*, 103618. [[CrossRef](#)]
18. Yanhui, Z.; Hoteit, I.; Katterbauer, K.; Maucec, M.; Marsala, A.F. Feature-based Ensemble History Matching in A Fractured Carbonate Reservoir Using Time-Lapse Deep Electromagnetic Tomography. *J. Petrol. Sci. Eng.* **2022**, *208*, 109259.
19. Carrigan, C.R.; Xianjin, Y.; LaBrecque, D.J.; Larsen, D.; Freeman, D.; Ramirez, A.L.; Daily, W.; Aines, R.; Newmark, R.; Friedmann, J.; et al. Electrical Resistance Tomographic Monitoring of CO₂ Movement in Deep Geologic Reservoirs. *Int. J. Greenh. Gas. Control.* **2013**, *18*, 401–408. [[CrossRef](#)]
20. Coulouma, G.; Lagacherie, P.; Samyn, K.; Grandjean, G. Comparisons of Dry ERT, Diachronic ERT and the Spectral Analysis of Surface Waves for Estimating Bedrock Depth in Various Mediterranean Landscapes. *Geoderma* **2013**, *199*, 128–134. [[CrossRef](#)]
21. Schmidt-Hattenberger, C.; Bergmann, P.; Bosing, D.; Labitzke, D.; Moller, M.; Schroder, S.; Wagner, F.; Schutt, H. Electrical Resistivity Tomography (ERT) for Monitoring of CO₂ Migration—From Tool Development to Reservoir Surveillance at the Ketzin Pilot Site. *Energy Procedia* **2013**, *37*, 4268–4275. [[CrossRef](#)]
22. Auken, E.; Doetsch, J.; Fiandaca, G.; Christiansen, A.V.; Gazoty, A.; Cahill, A.G.; Jakobsen, R. Imaging Subsurface Migration of Dissolved CO₂ in a Shallow Aquifer Using 3D Time-Lapse Electrical Resistivity Tomography. *J. Appl. Geophys.* **2014**, *101*, 31–41. [[CrossRef](#)]
23. Keck, L.J.; Schuster, C.L. Shallow Formation Hydrofracture Mapping Experiment. *J. Pressure Vessel Technol.* **1978**, *100*, 24–27. [[CrossRef](#)]
24. Jincheng, Z. Monitoring Technique Based on the Electrometric Method Interwell. *Seismol. Geol.* **2001**, *2*, 292–300.
25. Anlin, X. Borehole-Surface Resistivity Tomography and It's Application in Faults Detection on Beishan. Master's Thesis, Nanjing University, Nanjing, China, 2014.
26. Shen, J.S.; Wang, Z.G.; Ma, C. Application of The Cross-Hole Electromagnetic Method(CHEM) in Hydrocarbon Reservoir Monitoring. *Oil Geophys. Prospec.* **2014**, *49*, 213–224.
27. Nwufoh, P.; Hu, Z.; Wen, D.; Wang, M. Nanoparticle Assisted EOR during Sand-Pack Flooding: Electrical Tomography to Assess Flow Dynamics and Oil Recovery. *Sensors* **2019**, *19*, 3036. [[CrossRef](#)]

28. Ehsan, H.; Moseni, A.A. Garau Formation as an Unconventional Hydrocarbon Resource in Southwestern Iran: A Geochemical Investigation. *J. Pet. Explor. Prod. Technol.* **2023**, *13*, 1535–1549.
29. Lai, J.; Wang, G.; Fan, Q.; Pang, X.; Li, H.; Zhao, F.; Li, Y.; Zhao, X.; Zhao, Y.; Huang, Y.; et al. Geophysical Well-Log Evaluation in the Era of Unconventional Hydrocarbon Resources: A Review on Current Status and Prospects. *Surv. Geophys.* **2022**, *43*, 913–957. [[CrossRef](#)]
30. Muther, T.; Qureshi, H.A.; Syed, F.I.; Aziz, H.; Siyal, A.; Dahaghi, A.K.; Negahban, S. Unconventional Hydrocarbon Resources: Geological Statistics, Petrophysical Characterization, and Field Development Strategies. *J. Pet. Explor. Prod. Technol.* **2021**, *12*, 1463–1488. [[CrossRef](#)]
31. Wenfeng, H.; Hou, W.; Chen, L.; Huang, H.; Ebey, M.; Cheng, Y. Comprehensive Analysis on the Oil-Water Interface Distribution Characteristics in Tight Oil Reservoir. *Front. Energy Res.* **2022**, *10*, 858214.
32. Hu, Z.; Al-Ameri, L.; Gardy, J.; Alhreez, M.; Wen, D. In Situ Produced Nanoparticles at the Oil-Water Interface for Conformance Control and Enhanced Oil Recovery. *Energy Fuels* **2022**, *36*, 12986–12996. [[CrossRef](#)]
33. Zuoli, L.; Anirban, C.; Jessica, F.; Edgar, Z.; Flavio, V.; Zhenghe, X.; Qingxia, L.; Cesar, F.; William, C.M. Study on Demulsifier Crude Oil Interactions at Oil-Water Interface for Crude Oil Dehydration. *Colloid Surface A* **2021**, *630*, 127526.
34. Wang, M.; Wang, Q.; Karki, B. Arts of Electrical Impedance Tomographic Sensing. *Philos. T. R. Soc. A* **2016**, *374*, 0329. [[CrossRef](#)] [[PubMed](#)]
35. Wang, Q.; Jia, X.; Wang, M. Bubble Mapping: Three-Dimensional Visualisation of Gas–Liquid Flow Regimes Using Electrical Tomography. *Meas. Sci. Technol.* **2019**, *30*, 045303. [[CrossRef](#)]
36. Wang, M. Inverse Solutions for Electrical Impedance Tomography Based on Conjugate Gradients Methods. *Meas. Sci. Technol.* **2002**, *13*, 101–117. [[CrossRef](#)]
37. Wu, X. The Reseaching of Applying the Well ERT Technology at the Reservoir of Low Porosity and Low Percolation of Yanhewan Oil Region. Master’s Thesis, Chang’an University, Xi’an, China, 2008.
38. He, Y.; Qin, J.; Cheng, S.; Chen, J. Estimation of Fracture Production and Water Breakthrough Locations of Multi-Stage Fractured Horizontal Wells Combining Pressure-Transient Analysis and Electrical Resistance Tomography. *J. Petrol. Sci. Eng.* **2020**, *194*, 107479. [[CrossRef](#)]
39. Lindsay, K.A.; Rosenberg, J.R.; Tucker, G. From Maxwell’s Equations to the Cable Equation and Beyond. *Prog. Biophys. Mol. Bio.* **2003**, *85*, 71–116. [[CrossRef](#)]
40. Wang, M. Electrode Models in Electrical Impedance Tomography. *J. Zhejiang Univ. Sci. A* **2005**, *6*, 1386–1393. [[CrossRef](#)]
41. Chao, G.; Gray, K.E. A Coupled Geomechanics and Reservoir Simulator with A Staggered Grid Finite Difference Method. *J. Petrol. Sci. Eng.* **2022**, *209*, 109818.
42. Wentao, Z.; Xiang, R.; Hui, Z.; Hairong, Z.; Siwei, H.; Weixin, D. Generalized Finite Difference Method (GFDM) Based Analysis for Subsurface Flow Problems in Anisotropic Formation. *Eng. Anal. Bound. Elem.* **2022**, *140*, 48–58.
43. Lipan, L. Simulation for Radioactive well Logging in Fractured and Cavernous Carbonate Formation. Master’s Thesis, Jilin University, Changchun, China, 2020.
44. Song, H.; Weinan, L.; Yingming, L.; Kun, L. Acoustic Logging Response Law in Shales Based on Petrophysical Model. *Petrol. Sci.* **2022**, *19*, 2120–2130.
45. Bing, W.; Li, W.; Lu, J.; Wujun, J.; Song, H. Study on Acoustic Logging Response of Fractured Reservoirs Using a Novel Equivalent Medium Model. *Acta Geophys.* **2022**, *70*, 2695–2704.
46. Yang, R.; Liu, W.; Meng, L. Multifractal Analysis of the Structure of Organic and Inorganic Shale Pores Using Nuclear Magnetic Resonance (NMR) Measurement. *J. Mar. Sci. Eng.* **2023**, *11*, 752. [[CrossRef](#)]
47. Simon, S.; Pierrard, X.; Sjoblom, J.; Geir, H. Sorland. Separation Profile of Model Water-in-Oil Emulsions Followed by Nuclear Magnetic Resonance (NMR) Measurements: Application Range and Comparison with a Multiple-Light Scattering Based Apparatus. *J. Colloid Interf. Sci.* **2011**, *356*, 352–361. [[CrossRef](#)] [[PubMed](#)]
48. Lin, Q.J.; Shen, K.Y.; Jiang, Y.F.; Luo, Q.; Yao, J.; Tao, C.C. Application of Coiled Tubing Distributed Optical Fiber Logging Technology in Production Profile. *Well Text* **2023**, *32*, 58–62.
49. Qing, L.; Haoquan, W. Application Research of Optical Fiber Sensor in Petroleum Logging. *Petrochem. Ind. Technol.* **2022**, *29*, 62–64.
50. Paul, E.; Elisabeth, P. Well Testing of Radial Jet Drilling Wells in Geothermal Reservoirs. *Computat. Geosci.* **2022**, *26*, 1449–1463.
51. Abdullin, A.I.; Shamsiev, M.N.; Khairullin, M.K. Numerical Well Test Analysis of Fractured Porous Reservoirs with Consideration of Stress-Sensitivity Effect. *Lobachevskii J. Math.* **2021**, *42*, 2077–2081. [[CrossRef](#)]
52. Hashmi, G.M.; Kabir, C.S.; Hasan, A.R. Estimating Reliable Gas Rate with Transient-Temperature Modeling for Interpreting Early-Time Cleanup Data During Transient Testing. *J. Petrol. Sci. Eng.* **2015**, *133*, 285–295. [[CrossRef](#)]
53. Kuchuk, F.J. Interval Pressure Transient Testing with MDT Packer-Probe Module in Horizontal Wells. *Spe. Reserv. Eval. Eng.* **1998**, *1*, 509–518. [[CrossRef](#)]
54. Suzuki, A.; Niibori, Y.; Fomin, S.A.; Chugunov, V.A.; Hashida, T. Fractional Derivative-Based Tracer Analysis Method for the Characterization of Mass Transport in Fractured Geothermal Reservoirs. *Geothermics* **2015**, *53*, 125–132. [[CrossRef](#)]
55. Lu, Z.; Jia, Y.; Cheng, L.; Pan, Z.; Xu, L.; He, P.; Guo, X.; Ouyang, L. Microseismic Monitoring of Hydraulic Fracture Propagation and Seismic Risks in Shale Reservoir with a Steep Dip Angle. *Nat. Resour. Res.* **2022**, *31*, 2973–2993. [[CrossRef](#)]

56. Rastegaev, A.V.; Chernykh, I.; Ponomareva, I.N.; Martyushev, D. Assessment of Results of Hydraulic Fracturing on the Basis of Microseismic Monitoring, Geological and Production Data Comprehensive Analysis. *Oil Indus. J.* **2019**, *8*, 122–125. [[CrossRef](#)]
57. Wang, X.J.; Feng, L. Orientation Determination of High Permeability Zone with Borehole-to-Surface Potentiometric Method. *J. China Univ. Pet.* **2006**, *5*, 67–70.
58. Li, G.; Liu, D.; Wang, N. Application of Well-ground Potential Image in Regional Evaluating of Changqing Oilfield. *Well Logging Technol.* **2019**, *43*, 323–328.
59. Li, G.; Kong, Q.; Zeng, Y. Application of Borehole-Surface Electrical Imaging Logging Technology for Evaluating Reservoirs in Y Oilfield in Muglad Basin. *Well Logging Technol.* **2020**, *44*, 77–81.
60. Tan, H.Q.; Shen, J.S.; Zhou, C.; Dong, H. Borehole-to-Surface Electrical Imaging Technique and its Application to Residual Oil Distribution Analysis of the Eighth Section in Gudong Oilfield. *J. Univ. Pet. China* **2004**, *2*, 31–37.
61. Cai, S.Q.; Ye, Y.P.; Zou, L.X.; Zhou, J.Y.; Sheng, Y.X. Application of Well Ground Potential Image in Residual Oil Evaluation of Wu1 Block, Xingjiang Oilfield. *Spec. Oil Gas Reserv.* **2005**, *5*, 55–58+65–107.
62. Wang, W.; Guo, W.G.; Wang, G.Q.; Chen, W.W.; Fang, Y.J.; Yao, J.R. Application of Borehole-surface Electrical Imaging in Qiuling Oilfield, Tuha Basin. *Well Logging Technol.* **2008**, *3*, 267–271.
63. Xu, X. Application of Well-Ground Potential Image in Daqing Oil Field. Master's Thesis, China University of Geosciences, Beijing, China, 2009.
64. Fei, W.; Ming, C. Favorable Area Prediction of Chang 8 Reservoir in Chi 46 Well Area of Jiyuan Oil Field. *Liaoning Chem. Ind.* **2012**, *41*, 573–575.
65. Lu, B. The Application of Borehole-to-Surface Potential Imaging Technique in Residual Oil Distribution Analysis. *Petrol. Tub. G. Ins.* **2012**, *26*, 61–63.
66. Li, L. The Application of Borehole to Surface Potential Imaging Technique in Residual Oil Distribution in Area K. Master's Thesis, Northeast Petroleum University, Daqing, China, 2017.
67. Yang, Y. The Prediction of Favorable Reservoir Area Based on Borehole-Tosurface Potential Imaging Technique. Master's Thesis, Xi'an Shiyou University, Xi'an, China, 2020.
68. Yang, W.; Shiqing, C.; Kaidi, Z.; Luis, F.A. Investigation on The Transient Pressure Response of Water Injector Coupling the Dynamic Flow Behaviors in The Wellbore, Waterflood-Induced Fracture and Reservoir: Semi-Analytical Modeling and A Field Case. *Int. J. Heat. Mass. Tran.* **2019**, *130*, 668–679.
69. Wang, Y.; Cheng, S.Q.; Zhang, K.D.; He, Y.W.; Yu, H.Y. Pressure-Transient Analysis of Water Injectors Considering the Multiple Closures of Waterflood-Induced Fractures in Tight Reservoir: Case Studies in Changqing Oilfield, China. *J. Pet. Sic. Eng.* **2019**, *172*, 643–653. [[CrossRef](#)]
70. Wang, P. Zhuang 9 Well Area of Xifeng Oilfield Flood Developmient Well Pattern Adaptability Research. Master's Thesis, Xi'an Shiyou University, Xi'an, China, 2013.
71. Zhang, J.; Revil, A. Cross-well 4-D Resistivity Tomography Localizes the Oil–Water Encroachment Front during Water Flooding. *Geophys. J. Int.* **2015**, *201*, 343–354. [[CrossRef](#)]
72. Perri, M.T.; Cassiani, G.; Gervasio, I.; Deiana, R.; Binley, A. A Saline Tracer Test Monitored Via Both Surface and Cross-Borehole Electrical Resistivity Tomography: Comparison of Time-Lapse Results. *J. Appl. Geophys.* **2012**, *79*, 6–16. [[CrossRef](#)]
73. Yang, Q.; Tan, M.; Li, G.; Zhang, F.; Bai, Z. Numerical Simulation and Joint Inversion of Three-Dimensional Borehole to Surface Resistivity of High Deviated or Horizontal Wells. *Chin. J. Geophys.* **2020**, *63*, 4540–4552.
74. Ding, D. Research on Hydraulic Fracturing Monitoring Based on Surface-Borehole Potential Method. Master's Thesis, China University of Petroleum, Beijing, China, 2018.
75. Wu, Z. Application of the Borehole to Surface Electric Potential Image Technique to Monitoring Hydraulic Fractures of Coalbed Methane. *Coal Geol. Explor.* **2006**, *6*, 63–64.
76. Wu, B.; Li, J. Application of Monitoring Technology Based on the Electro-Metric Method Inter Well in Fracturing Monitoring. *Pet. Geol. Eng.* **2011**, *25*, 126–128.
77. Li, G.; Liu, Q.; Peng, T.S.; Yang, H.; Yu, X.; Liang, X.J. The Application and Reserch of Electrometric Method Test Technology on the Caboniferous Volcanicsuperficial Reservoir Hydraulic Fracturing. *Xinjiang Oil Gas.* **2012**, *8*, 69–74.
78. Wang, J. Research and Application of Borehole-Surface Electrical Resistivity Method of Monitoring Hydraulic Fracturing in the Oilfield Method of Monitoring Hydraulic Fracturing in the Oilfield. Master's Thesis, Jilin University, Changchun, China, 2013.
79. Yang, X. Research on Methods of Electric Potential Method Monitoring Fractring Fracture. Master's Thesis, China University of Petroleum, Beijing, China, 2016.
80. Wu, H.; Fu, P.; Yang, X.; Morris, J.P.; Johnson, T.C.; Settgest, R.R.; Ryerson, F.J. Accurate Imaging of Hydraulic Fractures Using Templated Electrical Resistivity Tomography. *Geothermics* **2019**, *81*, 74–87. [[CrossRef](#)]
81. He, Y.; Xu, Y.; Tang, Y.; Qiao, Y.; Yu, W.; Sepehrnoori, K. Multi-Phase Rate Transient Behaviors of the Multi-Fractured Horizontal Well with Complex Fracture Networks. *J. Energy Resour. Technol.* **2022**, *144*, 043006. [[CrossRef](#)]
82. He, Y.; Cheng, S.; Qin, J.; Chen, J.; Wang, Y.; Feng, N.; Yu, H. Successful Application of Well Testing and Electrical Resistance Tomography to Determine Production Contribution of Individual Fracture and Water-Breakthrough Locations of Multifractured Horizontal Well in Changqing Oil Field, China. In Proceedings of the SPE Annual Technical Conference and Exhibition, San Antonio, TX, USA, 9–11 October 2017.

83. Wang, Y.; Ayala, L.F. Explicit Determination of Reserves for Variable-Bottomhole-Pressure Conditions in Gas Rate-Transient Analysis. *SPE J.* **2020**, *25*, 369–390. [[CrossRef](#)]
84. Wang, Y.; Cheng, S.; Qin, J.; Lei, Z.; An, X.; Yu, H. Development Theory and Practice of Water Injection Induced Fractures in Ultra-Low Permeability Reservoirs. *Sci. Sin. Technol.* **2022**, *52*, 613–626. [[CrossRef](#)]
85. Wang, Y.; Cheng, S.; Zhang, F.; Feng, N.; Li, L.; Shen, X.; Li, J.; Yu, H. Big Data Technique in The Reservoir Parameters' Prediction and Productivity Evaluation: A Field Case in Western South China Sea. *Gondwana Res.* **2021**, *96*, 22–36. [[CrossRef](#)]
86. Liu, Y.C.; Yu, D.B.; Kong, W.F.; Shan, L.Q.; Sun, M.G. Dynamic Analysis of Cross-well Fracturing Based on Eccentric Potential Method. *J. Instrum. Autom. Syst.* **2022**, *5*, 21–26.
87. Johnson, T.C.; Burghardt, J.A.; Strickland, C.; Knox, H.; Vermeul, V.R.; White, M.D.; Schwering, P.; Blankenship, D.A.; Kneafsey, T.J. 4D Proxy Imaging of Fracture Dilatation and Stress Shadowing Using Electrical Resistivity Tomography during High Pressure Injections Into a Dense Rock Formation. *J. Geophys. Res-Sol. Earth* **2021**, *126*, e2021JB022298. [[CrossRef](#)]
88. Jiang, J. Well-Earth ERT Non-Polarized Electrodes Design and Performance Research. Master's Thesis, Jilin University, Changchun, China, 2013.
89. Stanley, S.J.; Bolton, G.T. A Review of Recent Electrical Resistance Tomography (ERT) Applications for Wet Particulate Processing. *Part. Part. Syst. Char.* **2008**, *25*, 207–215. [[CrossRef](#)]
90. Schlager, H.I.; Baas, J.H.; Wang, M.; Best, J.; Williams, R.A.; Peakall, J. Electrical Resistance Tomography for Suspended Sediment Measurements in Open Channel Flows Using a Novel Sensor Design. *Part. Syst. Char.* **2006**, *23*, 313–320. [[CrossRef](#)]
91. Wang, Q.; Polansky, J.; Wang, M.; Wei, K.; Qiu, C.; Kenbar, A.; Millington, D. Capability of Dual-Modality Electrical Tomography for Gas-Oil-Water Three-Phase Pipeline Flow Visualisation. *Flow. Meas. Instrum.* **2018**, *62*, 152–166. [[CrossRef](#)]
92. Wang, Q.; Jia, X.; Mi, W. Fuzzy Logic Based Multi-Dimensional Image Fusion for Gas–Oil–Water Flows With Dual-Modality Electrical Tomography. *IEEE T Instrum. Meas.* **2020**, *69*, 1948–1961. [[CrossRef](#)]
93. Hurry, R.J.; Mi, W.; Williams, R.A.; Cross, C. An Electrical Impedance Sensing System for Monitoring Hydraulic Flow Transport in Heap Leach Test Columns. In Proceedings of the 5th World Congress on Industrial Process Tomography, Bergen, Norway, 3–6 September 2007.
94. Sun, H. The Improvement and Implementation of Synchronization Technology of Borehole-Surface ERT System. Master's Thesis, Jilin University, Changchun, China, 2014.
95. Guo, T.R.; Tong, L.T.; Chiang, L.W.; Yang, C.H. A Fracture Study by Using Bipole–Bipole Cross-Well Logging. *J. Appl. Geophys.* **2011**, *75*, 203–210. [[CrossRef](#)]
96. Ochs, J.S.; Klitzsch, N. Considerations Regarding Small-Scale Surface and Borehole-to-Surface Electrical Resistivity Tomography. *J. Appl. Geophys.* **2020**, *172*, 103862. [[CrossRef](#)]
97. LaBrecque, D.; Birken, R.A.; LaBrecque, D. Design of a Multisource Capable, Hybrid Cabled/Distributed ERT/IP Data Acquisition System. In Proceedings of the SEG/AAPG/SEPM First International Meeting for Applied Geoscience & Energy, Denver, CO, USA, Online, 26 September–1 October 2021.
98. Wu, C.; Xu, T.H.; Xing, L.C.; Jia, N.H.; Lyu, W.F. Optimization of Electrode Array for Cross-hole ERT and Development of Monitoring Experimental System. *Com. Meas. Control.* **2023**, *9*, 1–11.
99. Zhang, Y. The Forward Modeling of Three-Dimensional Borehole-to-Surface Logging Technology. Master's Thesis, Ocean University of China, Qingdao, China, 2009.
100. Qu, Y. The 3-D Numerical Simulation and Inversion for Borehole-to-Ground Resistivity Survey & Dual Frequency Induced Polarization. Master's Thesis, China University of Geosciences, Beijing, China, 2008.
101. Wang, Z.; He, Z.; Wei, W. Study on Some Problems Upon 3D Modeline of DC Borehole-Ground Method. *Comput. Tech. Geophys. Geochem. Explor.* **2006**, *4*, 322–327.
102. Haili, Z.; Lijun, X.; Zhang, C.; Jinhai, H.; Xingbin, L. Image Reconstruction for Invasive ERT in Vertical Oil Well Logging. *Chin. J. Chem. Eng.* **2012**, *20*, 319–328.
103. Bouchedda, A.; Giroux, B.; Gloaguen, E. Bayesian ERT Inversion using Non-Stationary Inverse Matérn Covariance Matrix. In Proceedings of the 2015 SEG Annual Meeting, New Orleans, LA, USA, 18–23 October 2015.
104. Wang, C.; Li, S.; Liu, B.; Nie, L.; Zhang, F.; Song, J.; Guo, Q.; Ren, Y. 3D Constrained Electrical Resistivity Inversion Method Based on Reference Model. *Chin. J. Chem. Eng.* **2016**, *38*, 1685–1694.
105. Shishkina, O.A.; Indrupskiy, I.M.; Alekseeva, Y.V.; Makarova, A.A.; Kovalenko, K.V. Simulation of Time-Lapse Resistivity Logging during Two-Phase Well Testing in Petroleum Reservoirs. *J. Phys. Conf. Ser.* **2021**, *1730*, 012101. [[CrossRef](#)]
106. Kawtar, S.; Damien, J.; Roger, G.; Barthélémy, S.; Jean-Marie, H.; Louis, A.; Denis, V. A Data Mining Approach for Improved Interpretation of ERT Inverted Sections Using the DBSCAN Clustering Algorithm. *Geophys. J. Int.* **2021**, *225*, 1304–1318.

Disclaimer/Publisher's Note: The statements, opinions and data contained in all publications are solely those of the individual author(s) and contributor(s) and not of MDPI and/or the editor(s). MDPI and/or the editor(s) disclaim responsibility for any injury to people or property resulting from any ideas, methods, instructions or products referred to in the content.